Preliminary Design of
Advanced Quantum Beam Source
고도양자빔 이용시설 예비설계

한 국 원 자 력 연 구 소
Korea Atomic Energy Research Institute

31 / 47

Please be aware that all of the Missing Pages in this document were originally blank pages

제 출 문

한국원자력연구소장 귀하

본 보고서를 "중·저에너지 대용량 전자빔 조사시설 구축"에 관한 기술보고서로
제출합니다.

제목: Preliminary Design of Advanced Quantum Beam Source

2000년 7월

주저자: 이 병 철
공저자: 정 영 욱
　　　　조 성 오
　　　　박 성 희
　　　　이 종 민

국 문 요 약

초전도 가속기를 사용하는 고도양자빔 이용시설을 설계하였다. 고도양자빔 시설은 고출력 자유전자레이저, 단색 X-선 및 감마선, 중저에너지 전자빔, 대출력 펄스 중성자빔, 단색 양전자빔등, 기초과학과 산업분야의 다양한 연구에 이용될 수 있는 광양자 및 입자빔을 발생시키는 시설이다. 고도양자빔 이용시설의 설계는 CERN의 LEP가속기 해체 후에 SPS 초전도 가속기를 사용하는 것을 전제로 수행되었다.

ABSTRACT

The preliminary design of the Advanced Quantum Beam Source based on a superconducting electron accelerator is presented. The advanced quantum beams include: high power free electron lasers, monochromatic X-rays and γ-rays, high-power medium-energy electrons, high-flux pulsed neutrons, and high-flux monochromatic slow positron beam. The AQBS system is being re-designed, assuming that the SPS superconducting RF cavities used for LEP at CERN will be revived as a main accelerator of the AQBS system at KAERI, after the decommissioning of LEP at the end of 2000. Technical issues of using the SPS superconducting RF cavities for the AQBS project are discussed in this report. The advanced quantum beams will be used for advanced researches in science and industries.

TABLE OF CONTENTS

LIST OF TABLES

LIST OF FIGURES

1. Introduction and Motivation

The Korea Atomic Energy Research Institute (KAERI) is a national institute in researches and developments of atomic energy in Korea. Main interesting fields are focused in developments of nuclear reactors and nuclear fuels for power generation, production and application of radioactive isotopes, industrial applications of electron and/or proton accelerators, and future novel light sources. Among hundreds of projects at KAERI, the Advanced Quantum Beam Sources (AQBS) is one of the biggest projects for developing new light sources, from millimeter wavelength to γ-rays, as well as useful particle beam sources.

Free electron lasers (FELs) consist of an accelerator, an undulator, and an optical resonator. Ultrarelativistic beams, traveling sinusoidally in an alternating magnetic field, radiate coherent electromagnetic waves by the interaction between electron beams and optical fields. Because of nice features of a FEL, the radiation wavelength can be tuned continuously by changing the energy of electron beams and the strength of the magnetic field of the undulator. The average power of FELs can be generated up to several megawatts by using electron beams with average power of tens of megawatts. These distinguished advantages of FELs allow us to use FELs in many areas, such as, spectroscopy, laser medicine, surface physics, power beaming, photo chemical processes, and so on.

The AQBS enables us to produce other quantum beam sources in parallel with FEL light. High current electron, positron, and neutron beams can be generated for researches of nuclear physics and applications in industries. X-rays and γ-rays can be generated via Compton backscattering of electron beams with optical beams (FEL light or external laser light).

During 1990s, the mm-FEL and the FIR FEL were successfully lased at KAERI. To generate high average power FEL in a wider range of wavelength, the 2 MeV and 50 mA injector system was installed in 1998, in collaboration with BINP in Novosibirsk, Russia, and is being operational. The conceptual design using normal conducting RF cavity has been completed.

As the cost estimated from the previous design has been increased and the LEP Dismantling Project is actively in process, the usage of two 352 MHz SPS Superconducting (SC) cavities at KAERI has been seriously considered. By slightly modifying and upgrading the existing RF cavities in the injection system, the 352 MHz

SPS SC cavities allow us not only to reduce the cost and the time-scale but also to increase the energy of electron beam for IR and UV ranges of FEL wavelength. The AQBS project has been continued for last several years and is on-going with approved budget for next three years. With our budget and technical experience, the 352 MHz SPS SC cavities can survive at KAERI not only as a main accelerator but also as a first SC accelerator in Korea. The conceptual design of the AQBS project using 352 MHz SPS SC cavities are in progress and technical issues for modifications and upgrades are under discussion.

In this preliminary report, a brief overview of the AQBS Project at KAERI is presented in Chapter 2. In Chapter 3, the accelerator system, including the superconducting RF system of the linac and the cryogenic system, and beam diagnostics are briefly discussed. Possible advanced quantum beam sources at KAERI and their applications (which are main objectives of the AQBS project) are presented in Chapter 4, followed by Conclusion in Chapter 6.

2. Overview of the AQBS Project at KAERI

2.1 What is the AQBS ?

2.1.1 Integrated user facility of advanced quantum beams

The Advanced Quantum Beam Source (AQBS) is an integrated user facility that is dedicated for high-power photon beam and high-flux particle beam sources based on a high-current electron linear accelerator. The advanced quantum beam sources include:

- free electron lasers (FELs) from millimeter-wavelength to infrared
- monochromatic X-rays and γ-rays
- high power medium-energy electron beam
- high-flux pulsed neutron beam
- high-flux monochromatic slow positron beam

The concept of the AQBS is illustrated in Figure 2.1.1. Table 2.1.1 summarizes specifications of the quantum beam required for each application. The AQBS will enable users to perform various kinds of advanced researches in the field of nuclear industry and basic sciences.

The AQBS facility is based on a 100 MeV high-current electron accelerator and its schematic diagram is shown in Figure 2.1.2. The electron accelerator system consists of a 2 MeV injector, a 32-MeV main accelerator section, and three recirculation turns. The main accelerator section consists of two SPS superconducting accelerator modules, each of which has two four-cell 352 MHz superconducting RF cavities.
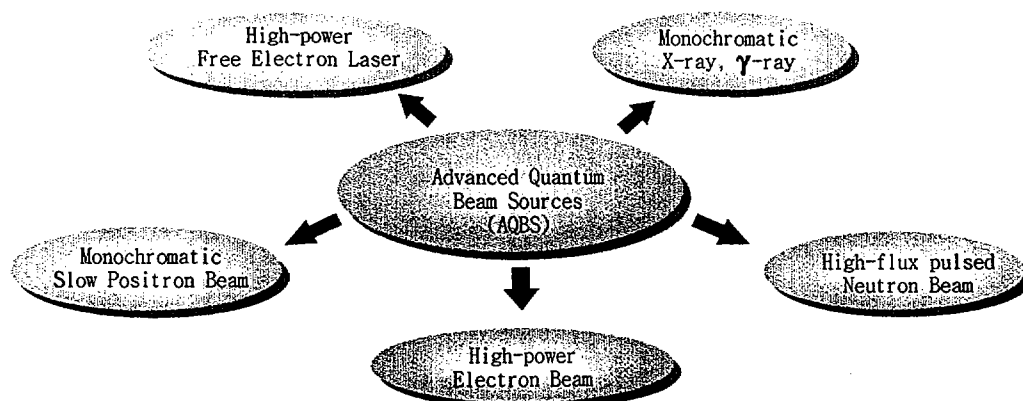
Figure 2.1.1 The concept of the Advanced Quantum Beam Source (AQBS)

3
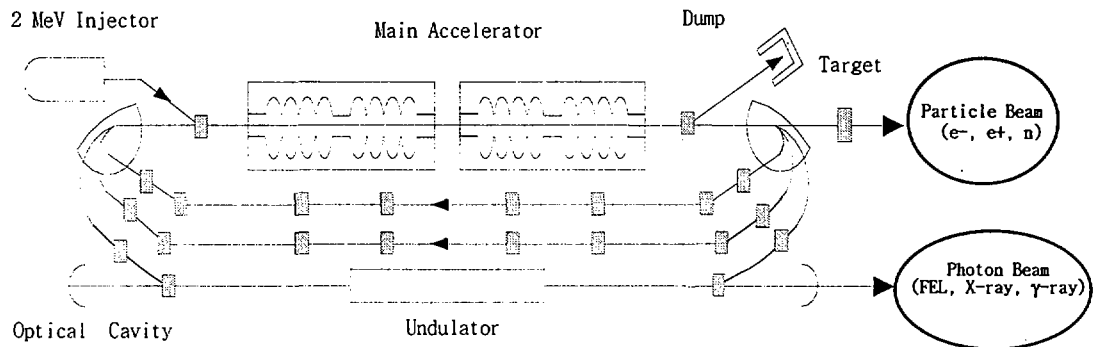
Figure 2.1.2 Schematic of the 100-MeV high-current electron accelerator.

Table 2.1.1 Specifications of the Advanced Quantum Beam Source

Quantum Beams	Specifications	Applications

FELs	- Wavelength range
	  * MMW FEL (3~10 mm)
	  * FIR FEL (90~300 μm)
	  * IR FEL (1~16 μm)
	- Average power: 1~5 kW*
		spectroscopy, materials processing, separation of stable isotopes, semiconductor and solid-state physics, biomedical researches, etc.

X-rays γ-rays	- Energy : 1~200 keV - Total flux : ~10^9 /sec - Energy resolution : 1~4 %	X-ray holography, lithography, nuclear resonance fluorescence, surface physics, etc.
Electrons	- Energy : 1~10 MeV - Average power : 100 kW	polymer processing, sterilization, power semiconductor, environmental protection, etc
Neutrons	- Energy : 50 keV ~ 2 MeV - Pulsewidth : ~ 30 ps - Total flux : 10^{14} n/se	nuclear data (neutron cross-section), neutron radiography, condensed matter physics, etc.
Positrons	- Energy : 10~100 eV - Total flux : ~ 10^7 e$^+$/sec - Pulsewidth : ~ 100 ps	material science, investigation of defects in metals and semiconductors, etc.

*: Expected average power at the IR FEL

4

The acceleration gradient of the superconducting RF cavity is 6 MV/m, and the energy gain per cavity is 8 MeV. Thus the energy gain per pass through the main acceleration section is 32 MeV. Therefore, we can get total energy of 98 MeV (= 2 MeV + 32 MeV x 3 turns) at maximum. The average current of the electron beam is 1~10 mA, depending on the applications and operation modes. Electron beams in this energy range with high intensity are attractive means to produce secondary radiation.

2.1.2 Free electron lasers

A free electron laser (FEL) is the most important project at AQBS. A relativistic electron beam enters an undulator (an apparatus generating periodic magnetic field) and it generates coherent electromagnetic radiation via the interaction with the optical fields. The wavelength of the radiation depends on the energy of the electron beam and the period of the undulator. The principle of operation of free electron lasers is demonstrated in Figure 2.1.3.
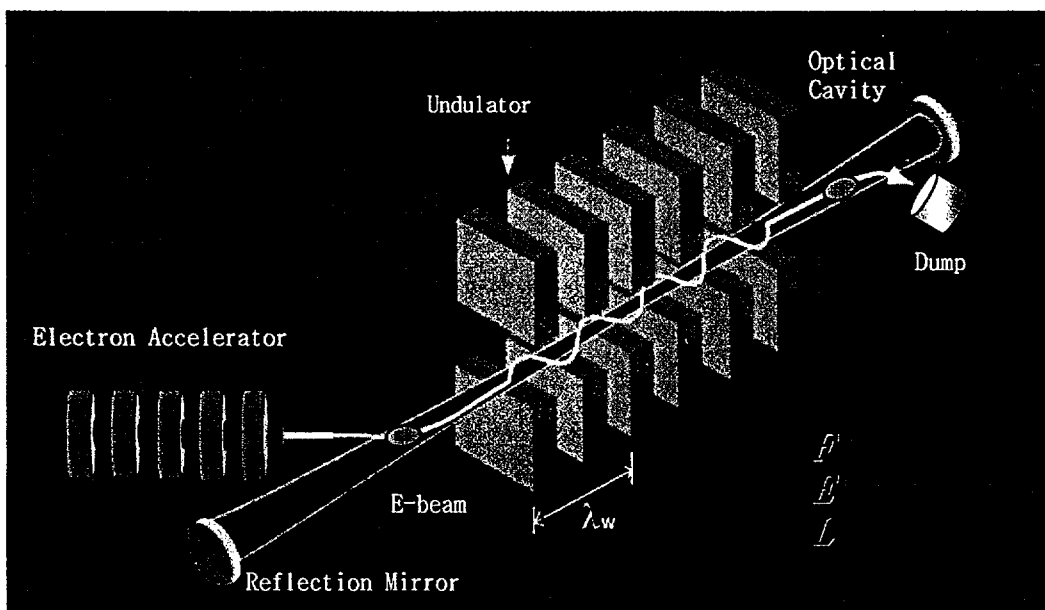
Figure 2.1.3 Principle of operation of free electron lasers.

KAERI has developed a millimeter-wave FEL since 1992 and a far-infrared FEL since 1996. The third one being developed is a high-power (1~5 kW) infrared FEL based on the 100 MeV high-current electron accelerator. Two FEL oscillators, having

5

different undulator parameters, will produce radiation with wavelengths of 5-16 μm and 1-5 μm respectively. The wavelength of the IR FEL can be extended further to visible and ultraviolet (UV) range via harmonic generation (typically, 3rd or 5th). The lasing of third harmonic in FELs has been demonstrated in the infrared FELs at JAERI and Jefferson Laboratory. Figure 2.1.4 shows the wavelength ranges of the three free electron lasers at KAERI.
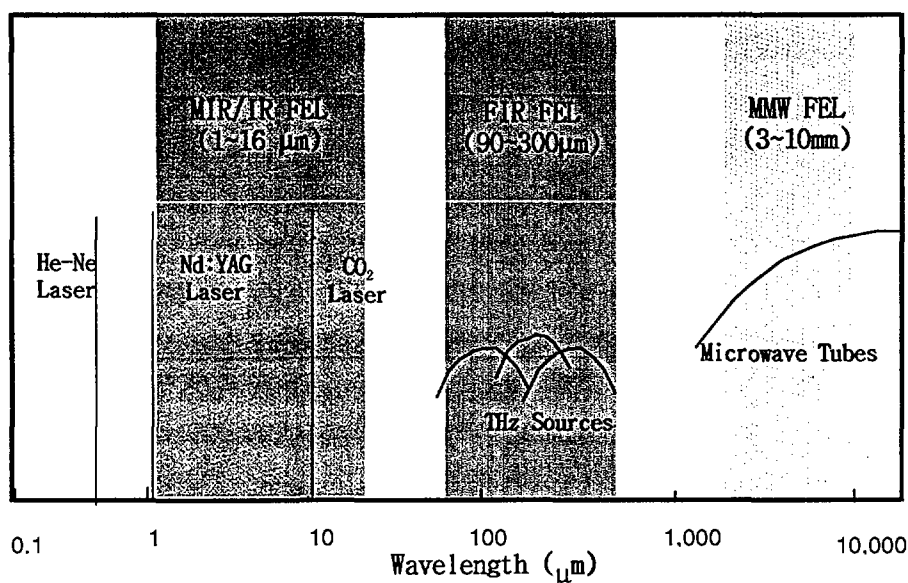
Figure 2.1.4 The tunable ranges of the free electron lasers at KAERI

The IR light will be short as much as 20 ps at a maximal repetition rate of 22 MHz with average power of 1~5 kW. Due to high level of average power, many industrial and scientific applications are promising. A wide-band IR FEL (Fourier limited, < 0.05 %) will enable users to research more precise spectroscopic studies of molecules, atoms, and solid-state materials. A wide tuning range of wavelength and narrow spectral width will enable the study of multi-photon dissociation (MPD) process of molecules. One of the applications of MPD is the separation of stable isotopes, such as, B^{10}, Si^{28}, Si^{30}, C^{13}, O^{18}, N^{15}, and so on. Those photon beams will open an opportunity in bio-medical researches, where the characteristic response of molecules and radicals to long-wavelength radiation is important, and in solid state physics, where the energy of IR photons corresponds to the characteristic excitation levels of semiconductor quantum-structures.

2.1.3 Monochromatic X-ray and γ-ray sources

Quasi-monochromatic X-rays will be produced in a small forward cone via Compton backscattering of laser light from relativistic electrons. Two schemes of Compton backscattering are being considered. One is using an external laser (external laser mode) and the other is using a FEL (FEL mode). A CW mode-locked Nd:YLF laser or a UV N_2 laser will be used in the external laser mode. The energy range of X-rays in the external laser mode is 20 ~ 180 keV for Nd:YLF laser, and 20 ~ 500 keV for UV N_2 laser. A schematic of the external laser mode is shown in Figure 2.1.5. In the FEL mode, the energy of the X-rays will range from 1 keV to 200 keV. Total flux of X-rays will be an order of 10^6~10^9 photons/sec, depending on the modes of operation. The energy resolution at full-width half maximum (FWHM) will be 1~4 %.

The monochromatic X-rays can be used for many advanced researches, such as, holography of living biological tissues, lithography, atomic inner-shell spectroscopy, nuclear resonance fluorescence, and so on. Monochromatic X-rays with energy of few tens of keV are especially well suited for the detailed study of radiation damage in biological systems caused by any kind of radiation since they allow to precisely quantify the energy deposition in cells and tissues.
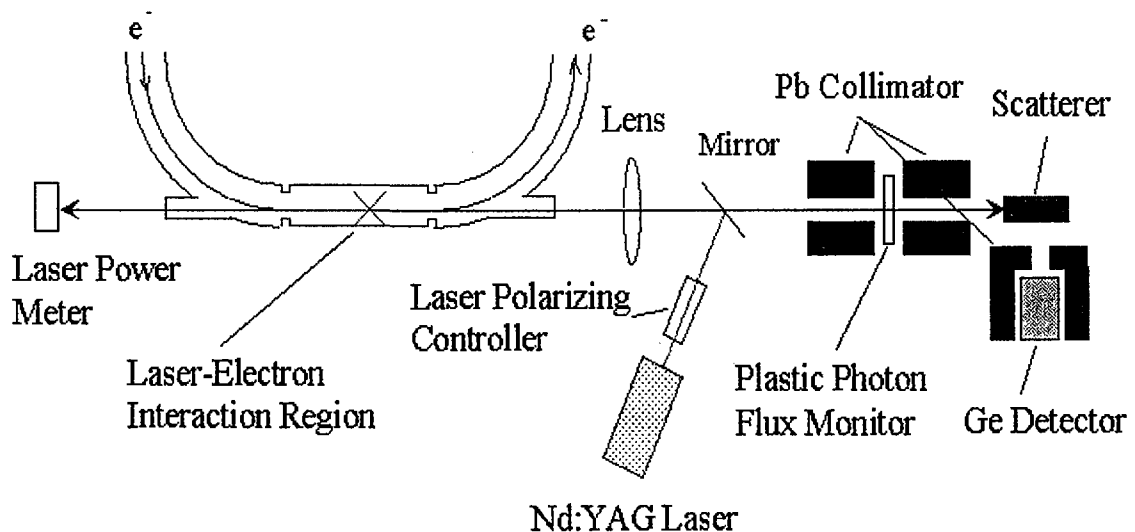
Figure 2.1.5 Schematic of the external laser mode of Compton backscattering.

2.1.4 Medium-energy electron beam source for e-beam processing

The electron beams in medium energy range (1~10 MeV) can be used directly to modify the molecular structure of various materials, such as, polymers, metals, films, semiconductors, and so on.

Polymerization is a well-known application of electron beam processing, in which several individual groups of molecules combine together to form one large group, called a polymer. This causes significant changes of physical properties of materials being treated and results in novel materials with many desirable physical characteristics, such as, high gloss and abrasion resistance. E-beam processing is an efficient way to initiate the polymerization process in many materials.

Crosslinking is a process by which an interconnected network of chemical bonds or links develops between large polymer chains and forms a stronger molecular structure. For example, when a product like plastic film or rubber substrate is treated with electrons, the large polymers in this product develop many linking bonds. These bonds increase the performance of this product and its resistance to weakening at elevated temperatures.

EB sterilization is a process of destroying contaminating microorganisms, by rendering them sterile or unable to reproduce. This occurs when electrons are irradiated directly into the microorganisms and break the DNA chains that control reproduction. Once a product has been sterilized, no microbial decomposition can take place. Since electrons act as a physical sterilizing agent rather than a chemical one, they do not change the chemical properties of the target materials or leave any residual chemicals. EB sterilization offers a number of advantages over chemical sterilization techniques, such as, those that use hydrogen peroxide and ethylene oxide.

Beamlines and irradiation ports of medium-energy electron beams, which are dedicated to these applications, are being designed. Since the average current of the electron beam is high enough (10 mA @ 10 MeV), a lot of useful applications that need high level of irradiation dose would be possible.

The parameters of the medium-energy electron beam are as follows:

- Energy : 1~10 MeV
- Average current : 50 mA @1~2 MeV, 10 mA @ 10 MeV
- Average beam power: 100 kW at maximum
- Pulse width : ~ 30 ps
- Repetition rate : 22.5 MHz at maximum.

2.1.5 High flux pulsed neutron beams

Neutrons can be produced from electron-induced bremsstrahlung by hitting a high-atomic-number radiator. In case of a radiator acting as a beam stop, bremsstrahlung is effectively converted into white neutron spectrum via (γ,n)-reactions. It ranges from a few eV up to the electron-beam energy reduced by the neutron binding energy.

Neutron yield depends on the type of target material as well as the beam energy and current. Typical neutron yield is about 7.56×10^{-3} n/s with a single 35 MeV electron impinging on Pb target. Thus it is possible to produce 1.41×10^{14} n/s from Pb target by colliding an electron beam of 3 mA average current at 35 MeV operating energy of the linac. The range of neutron spectra from evaporation process is 50 KeV~2 MeV. To get thermal spectrum, an assembly of moderator needs to be placed around the target.

The short pulse width (~ 30 ps) and the long pulse separation (~ 45 ns) of the AQBS electron beam allow to separate neutrons according to their energy with rather short flight paths. This allows detailed energy-dispersive studies of neutron interaction cross sections to be performed with small amounts of target materials.

The interaction of neutrons (in the keV and MeV range) in fuel with structural materials of fusion as well as fission reactors are processes of importance for the operation of such reactors and for the treatment of radioactive waste produced in them. The neutron radiation from AQBS will be used for the determination of relevant interaction cross sections. Another applications, such as, neutron radiography, condensed matter physics, and detection of explosives, are being considered.

2.1.6 High flux monochromatic slow positron beams

One of the secondary particle beams from the electron accelerator is a slow positron beam. A 100 MeV electron beam from the accelerator impinges on a target. As the electrons are decelerated in the target, they produce an intense flux of bremsstrahlung (literally, "braking radiation") photons. In turn, these photons interact with the electric fields of the nuclei in the target to produce electron-positron pairs. ·

The positrons and electrons emitted from the target are moderated by a set of tungsten vanes. Tungsten has a negative "work function" for positrons; positrons in the material are ejected from the surface with the energy distribution approximately equal to that of the electrons in the material. After the moderator vanes, the positrons are extracted into a beam by a combination of electric and magnetic fields. Figure 2.1.6 shows a schematic of the positron beam generator.

Total flux of slow positron beam generated by a 100 MeV and 1 mA electron beam is estimated to be 10^7 positrons per second. Advanced researches using the intense

positron beams are listed as follows: positron annihilation lifetime spectroscopy for probing defect density and size in metals or semiconductors, measurement of positronium lifetime for the study of phase transitions in liquid crystals and polymers, 2D angular correlation of the annihilation of γ-rays for the study of anisotropic momentum distribution of the conduction and valence electrons in semiconductors, and so on.
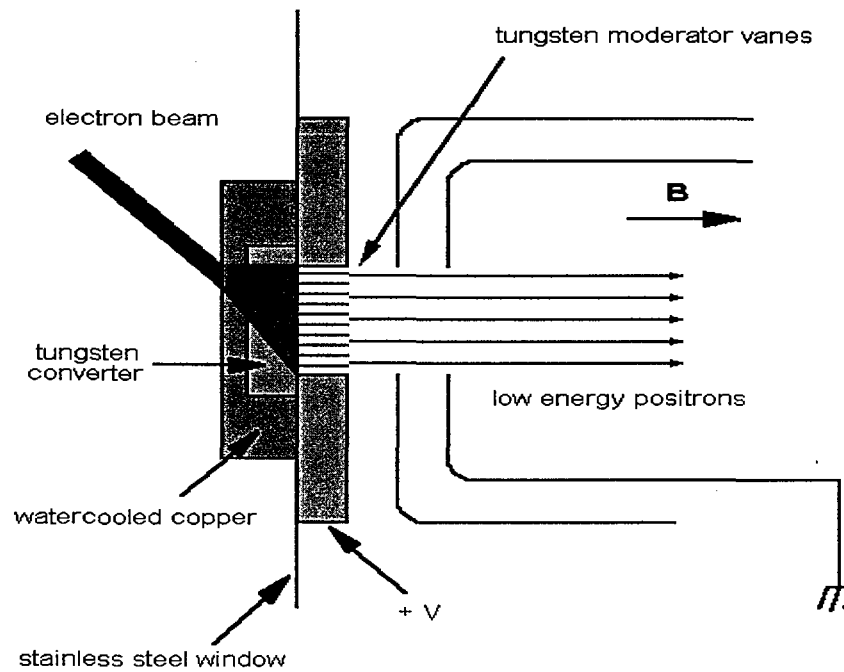
Figure 2.1.6 Schematic of the positron generator.

2.2 Current Status of the AQBS Project

2.2.1 Millimeter-wave FEL

In 1992, KAERI started to develop a millimeter-wave (MMW) free electron laser driven by a electrostatic accelerator and, at the end of 1994, KAERI succeeded in the lasing of the MMW FEL [2.2.1-2.2.4]. It was the second demonstration of successful lasing of the free electron laser driven by an electrostatic accelerator in the world. The range of the FEL wavelength is 3~10 mm. A compact permanent-magnet helical undulator was developed for the MMW FEL. Figure 2.2.1 shows a photograph of the KAERI MMW FEL and Table 2.2.1 summarizes the parameters of the KAERI millimeter-wave FEL.

The MMW FEL consists of a 30 keV electron gun, a 400 keV electrostatic acceleration column, a permanent-magnet helical undulator, a deceleration column, and a collector. After passing the undulator, the 'spent' electron beam is recirculated, *i.e.*, it is decelerated and captured by the collector. So the wall-plug efficiency is as high as 60%.

Table 2.2.1 Parameters of the KAERI millimeter-wave FEL

Electron beam	Energy	430 keV
	Current	2 A
	Emittance	20 π mm·mrad
	Pulsewidth	30 μs
Undulator	Type	Helical, permanent magnet
	Period	33 mm
	Number of period	28
	Magnetic field strength	1.33 kG
Radiation	Wavelength	3~10 mm
	Mode	TM_{11}
	Power	1 kW
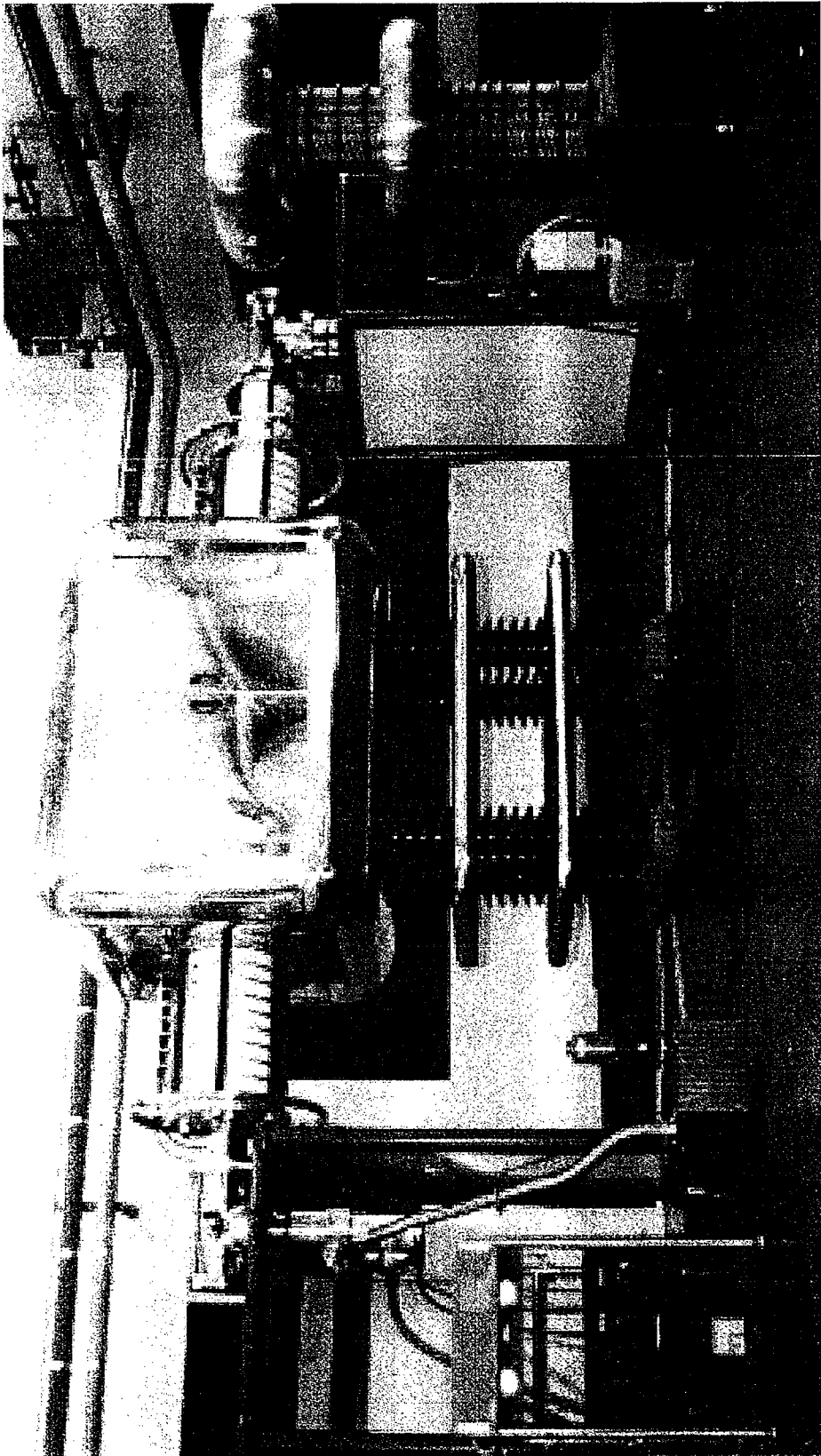
Figure 2.2.1 Photograph of the KAERI millimeter-wave free electron laser.

2.2.2 Far-infrared FEL

In 1996, KAERI started to develop a compact far infrared (FIR) FEL driven by a 7 MeV conventional microtron-type electron accelerator under the collaboration with the Budker Institute of Nuclear Physics, Russia [2.2.5-2.2.10]. Microtrons have many advantages as a driver of free electron lasers compared to RF linear accelerators. Since microtrons are compact and simple in structure, the microtron-based FELs become compact in size. Even though several research groups in the world have tried to get lasing of microtron-based FELs, there has been no successful demonstration of stable lasing.

Main difficulties come from intrinsically low peak current of the electron beam from microtrons. Since the FEL gain is proportional to peak current, it is not easy to get enough FEL gain from microtron-based FELs. Precise analysis of the losses in the optical cavity has been done to minimize the cavity losses. A low-loss waveguide-type optical cavity and a high-accuracy undulator have been developed. At the end of 1999, we successfully demonstrated the lasing of the microtron-based FIR FEL for the first time in the world. Figure 2.2.2 shows a photograph of the FIR FEL and Table 2.2.2 summarizes parameters of the FIR FEL.

The FIR FEL, including a pulsed modulator for RF generator, is compact such that it can be installed in a small (3m × 4m) room. The use of magnetron-type RF generator makes the system simple and cost-effective.

The undulator is a permanent magnet-assisted electromagnet. The strength of the magnetic field can be stronger than that of a hybrid-type undulator made of pure permanent magnets. It is tunable over a wide range simply by changing the electric current through the coil of the electromagnet. The use of permanent magnets together with electromagnet makes the spatial distribution of magnetic field uniform with high accuracy. The r.m.s error in the distribution of the magnetic field strength is less than 0.05%, which is much smaller than those of typical commercial undulators (~1%). Figure 2.2.3 shows a photograph of the undulator.

The wavelength of the FIR FEL is currently tunable over a range of 100-150 μm by changing the strength of the magnetic field over a range of 4.8~6.8 kG. The linewidth of the FIR FEL is 0.3% of central frequency. After upgrade of the microtron, the tunable range of the wavelength will be extended to 90~300 μm.

The far-infrared FEL will be used for various researches, such as, rotational spectroscopy of molecules, investigation of quantum devices, surface physics, development of non-destructive testing system, and so on.

Table 2.2.2 Parameters of the KAERI far-infrared FEL

Electron beam	Energy	6.5-7 MeV
	Current	40 mA (macropulse)
		1 A (micropulse)
	Energy spread	0.3 %
	Repetition rate	0.6~10 Hz (macropulse)
		2.8 GHz (micropulse)
	Pulsewidth	5 μs (macropulse)
		20 ps (micropulse)
Undulator	Type	Planar, Electromagnet
	Period	25 mm
	Number of period	80
	Magnetic field strength	4.8~6.8
FEL	Wavelength	100-150 μm (present) 90-300 μm
	Linewidth	0.3 %
	Power	1 kW (peak)
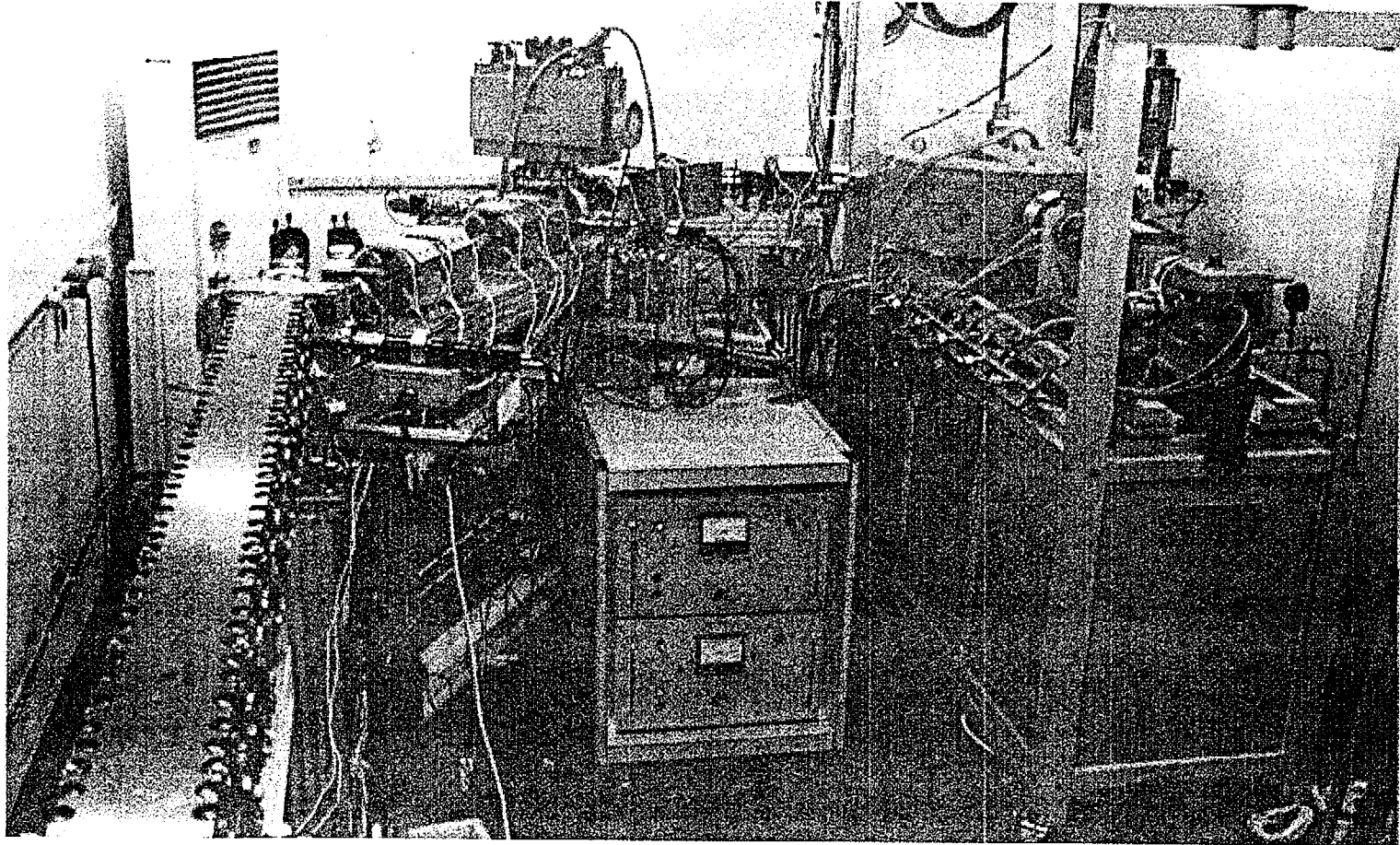
Figure 2.2.2 Photograph of the KAERI far-infrared free electron laser.
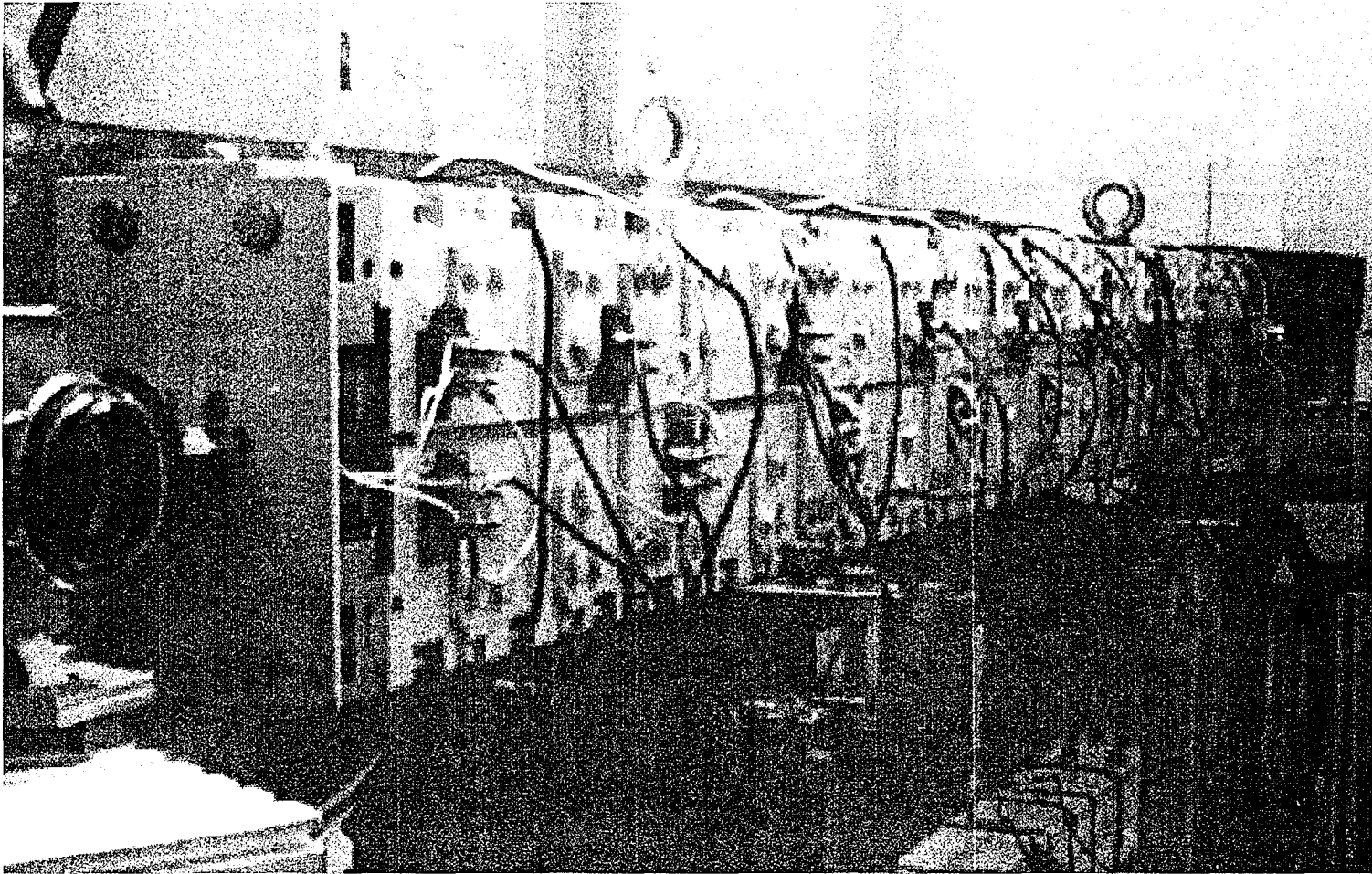
Figure 2.2.3 Photograph of the compact hybrid undulator for the KAERI FIR FEL.

2.2.3 High-current 2 MeV injector for the 100 MeV accelerator system

In parallel with the FIR FEL project, KAERI started another project of developing a 2 MeV high-current electron accelerator in 1997, which will be used as an injector for the AQBS system [2.2.11-2.2.12]. The injector has been designed and fabricated in collaboration with the Budker Institute of Nuclear Physics, Russia. The accelerator consists of a 300 keV electron gun, a RF bunching cavity, two main RF acceleration cavities, a 180 degree bending magnet, and a beam dump. Figure 2.2.4 shows a schematic diagram of the injector and Figure 2.2.5 shows a photograph of the injector. Figure 2.2.6 shows a photograph of the RF generator for the injector. The parameters of the 2 MeV injector for the 100 MeV accelerator are listed in Table 2.2.3.

Table 2.2.3 Parameters of the 2 MeV injector for the 100 MeV accelerator.

Electron energy (kinetic)	1.5 MeV (nominal) / 2.0 MeV (maximum)
Current	6 A (peak) / 45 mA (average)
Emittance	20π mm mrad
Repetition rate	up to 22.5 MHz
Pulse duration	350 ps
RF frequency	180 MHz
Operation mode	CW or pulsed

A pulsed electron beam is generated from the 300 keV electron gun. The maximum repetition rate of the electron beam is 22.5 MHz and its pulse width is 1.5 ns. After passing the RF bunching cavity, the pulse width is reduced to 350 ps. The resonance frequency of the RF cavities is 180 MHz. The cavity has copper clad stainless steel walls. The Q value of the cavity is 42,000, and the shunt impedance is 8.5 MΩ. The tuning range of the resonant frequency is 320 kHz, and the tuning speed is 5 kHz/sec. The wall loss at the cavity voltage of 850 kV is 100 kW. Total average output power of the tetrode-type RF generator is 260 kW.

The beam diagnostic system includes a beam position monitor, a DC current monitor, a pulse current monitor, and a beam profile monitor with a kicker magnet. The pulse current monitor measures the image charge due to pulse electron beam and its time resolution is 100 ps.

Anode Power Supply

RF Generator

Control System

300 kV P.S

Electron Gun

Buncher Cavity

Acceleration Cavity

Bending
Magnet
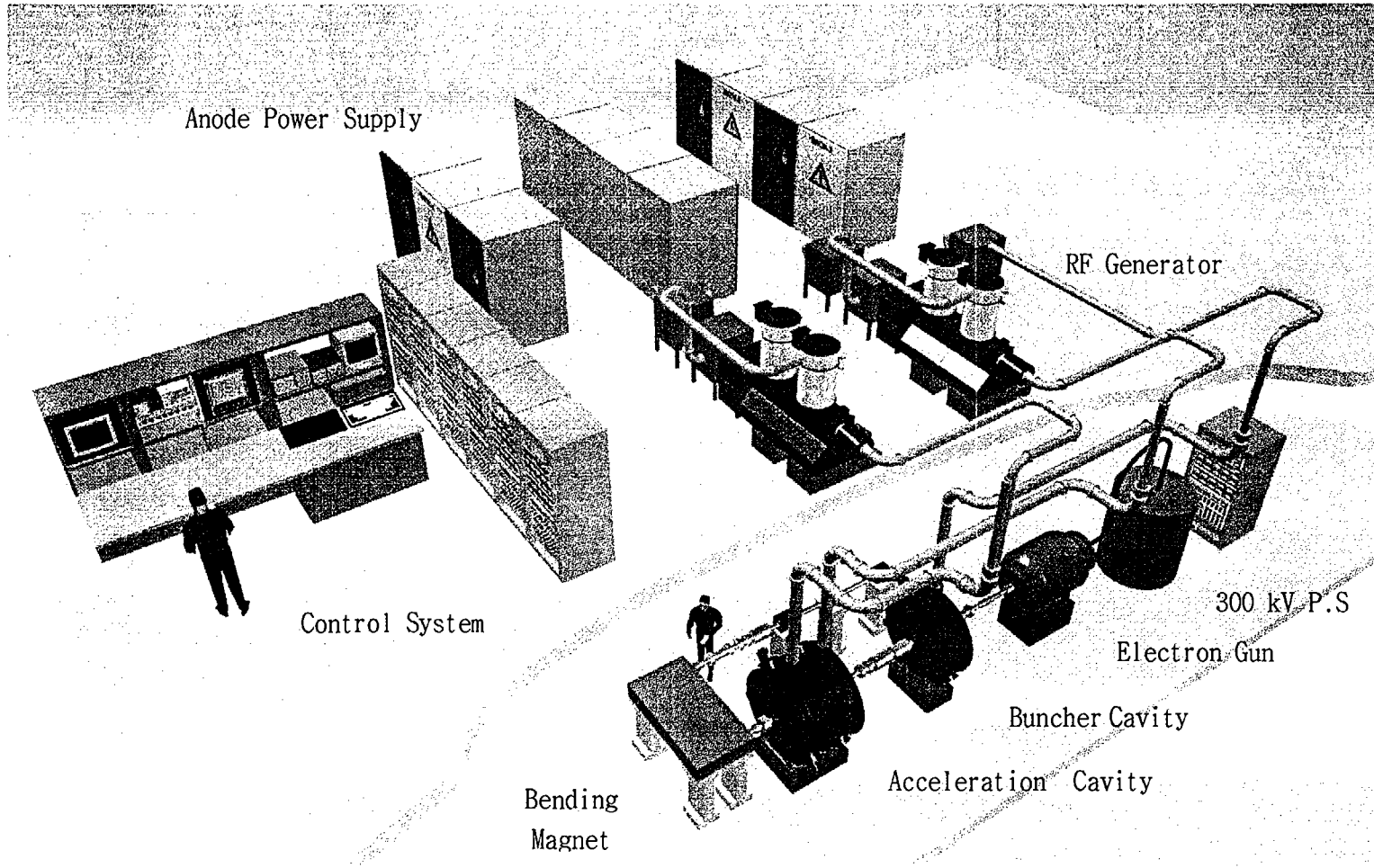
Figure 2.2.4 Artist's view of the 2 MeV injector system.
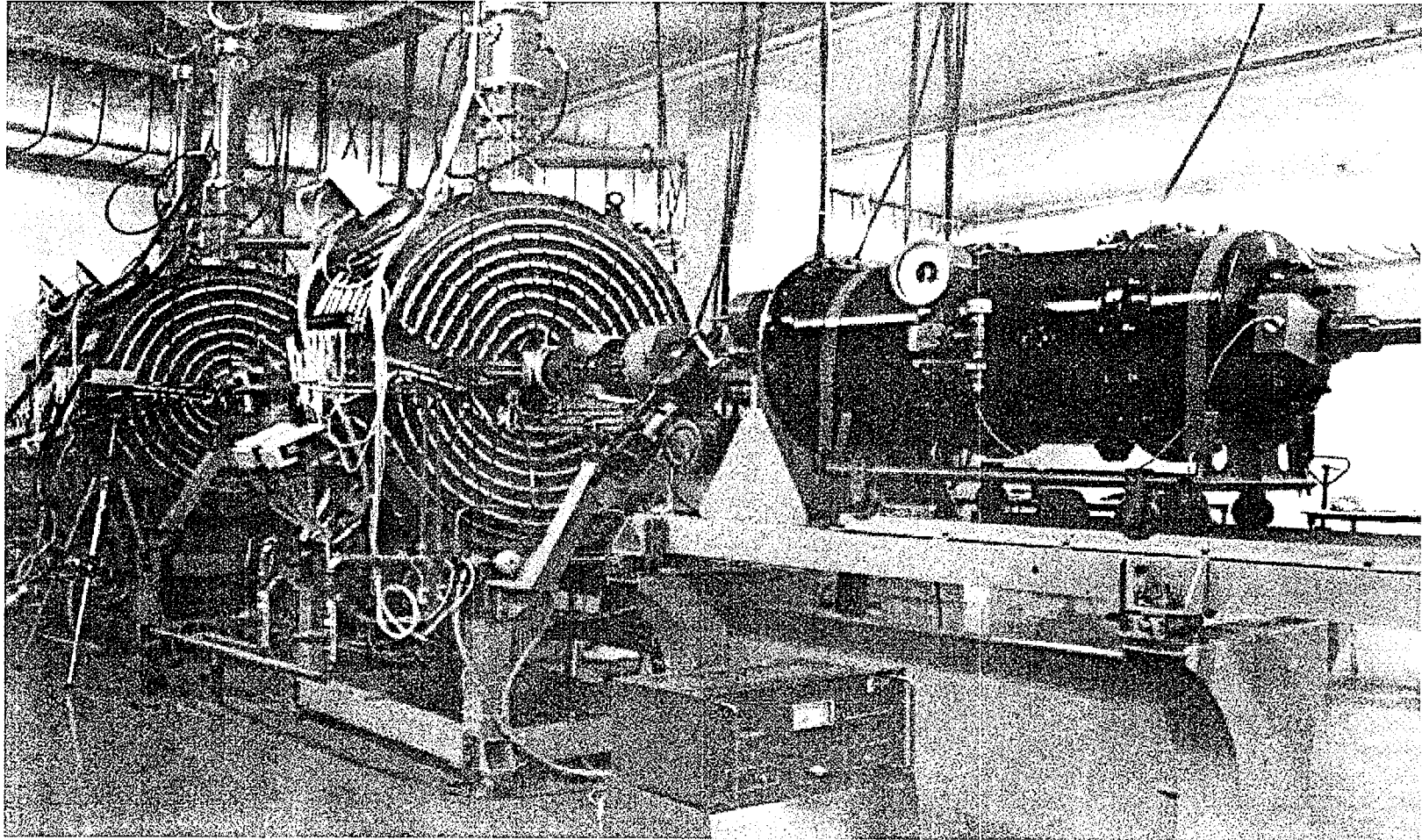
Figure 2.2.5 Photograph of the 2 MeV and 45 mA injector for the 100-MeV electron accelerator.
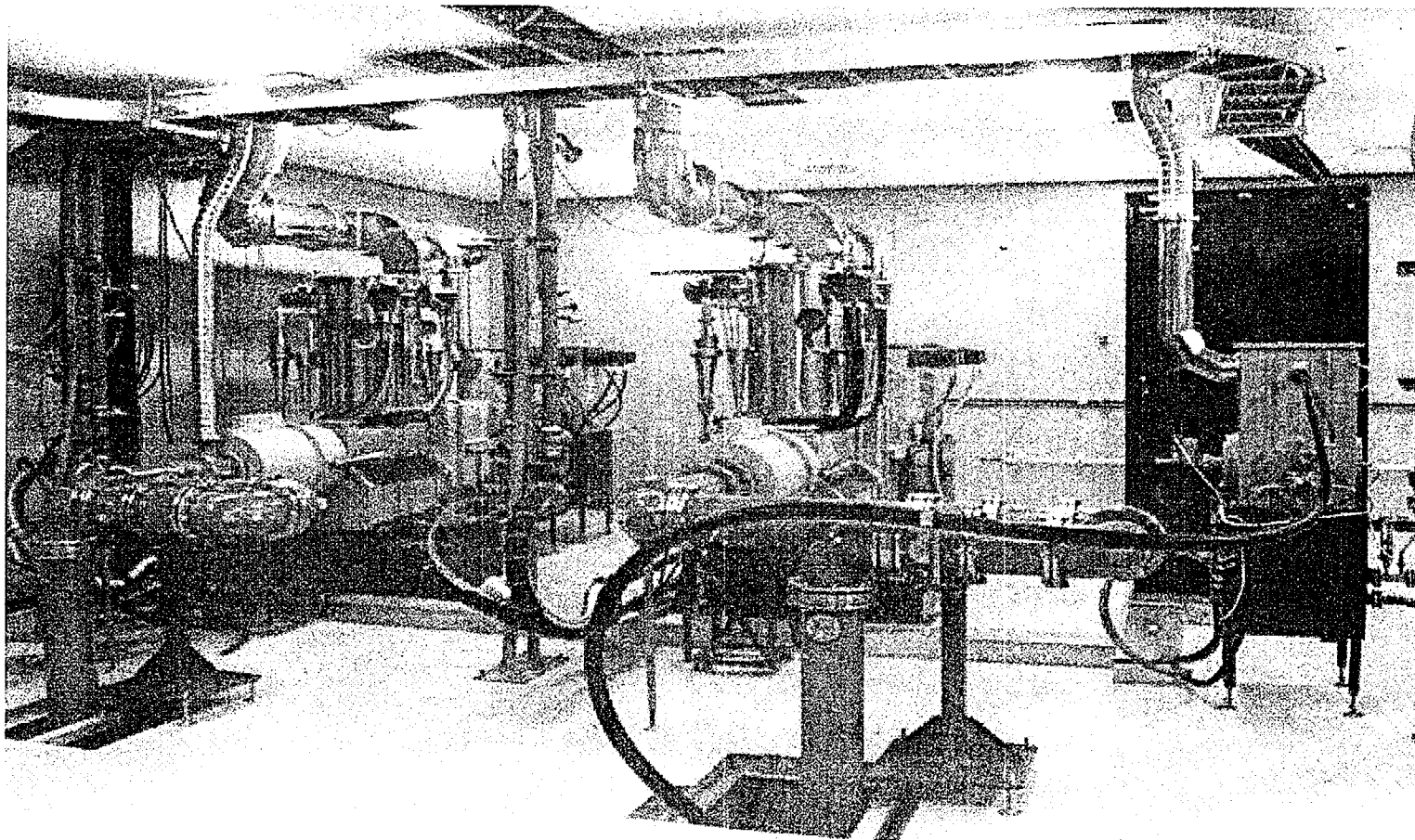
Figure 2.2.6 Photograph of the RF generator for the injector.
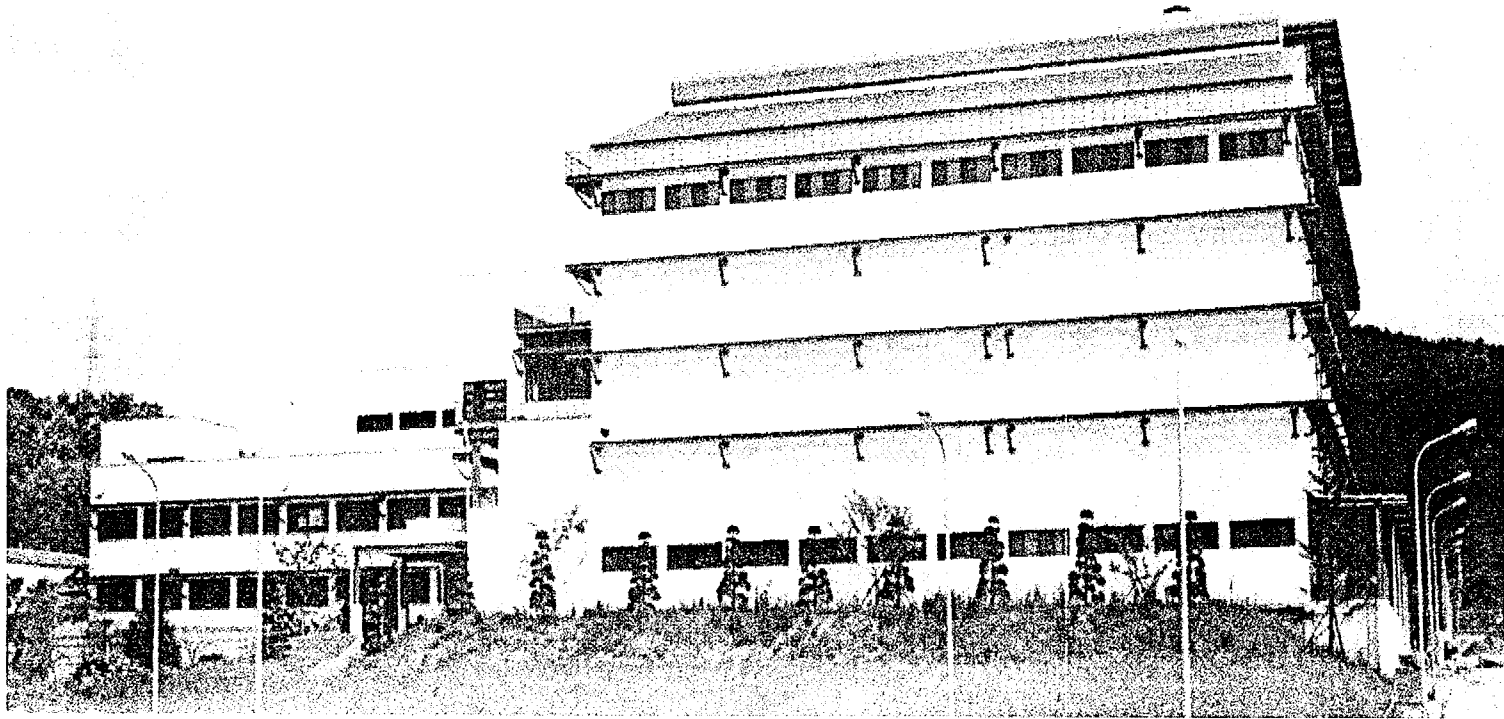
Figure 2.2.7 Photograph of the Engineering Research Building at KAERI.
The AQBS facility is placed in this building.
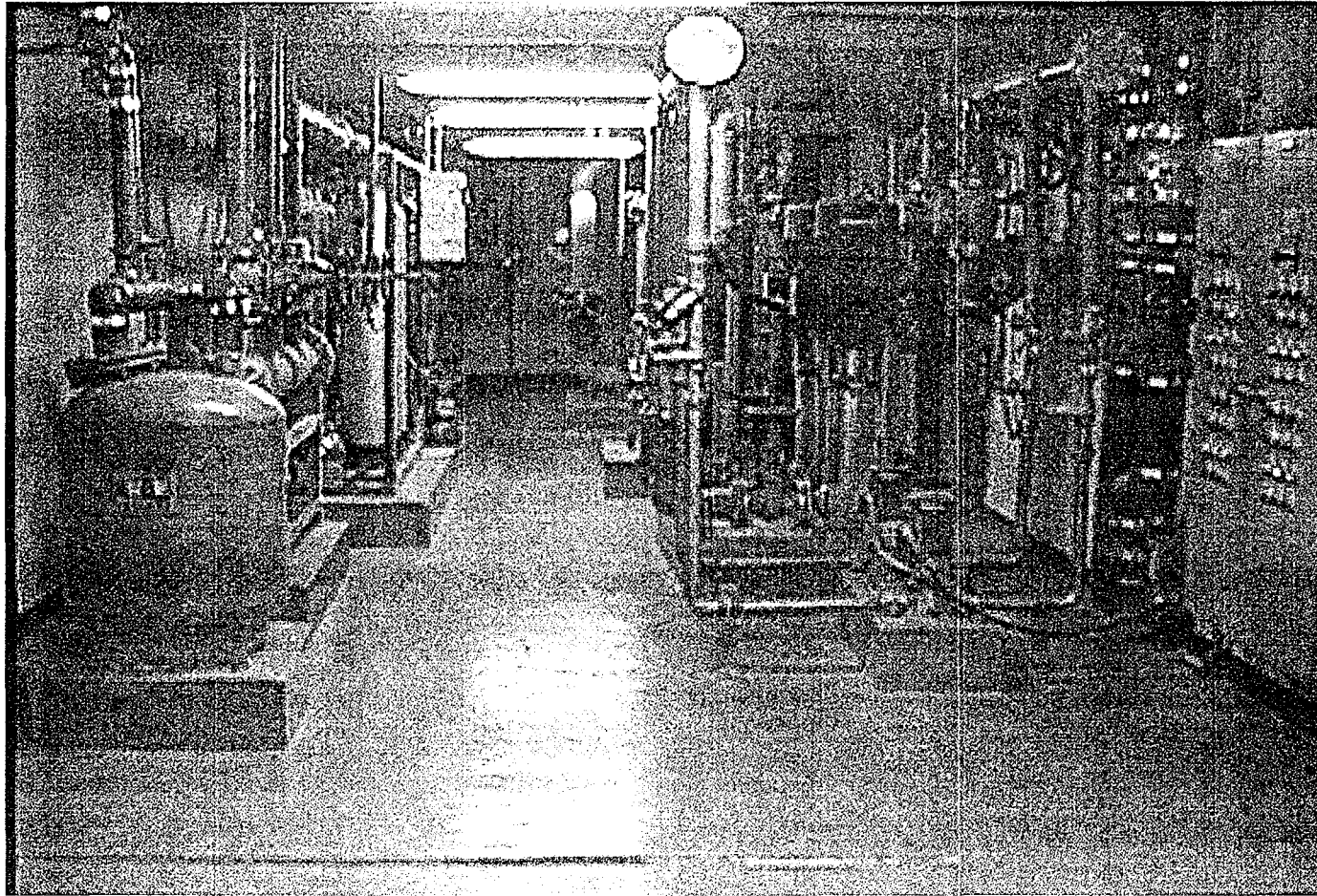
Figure 2.2.8 Photograph of the cooling water system.
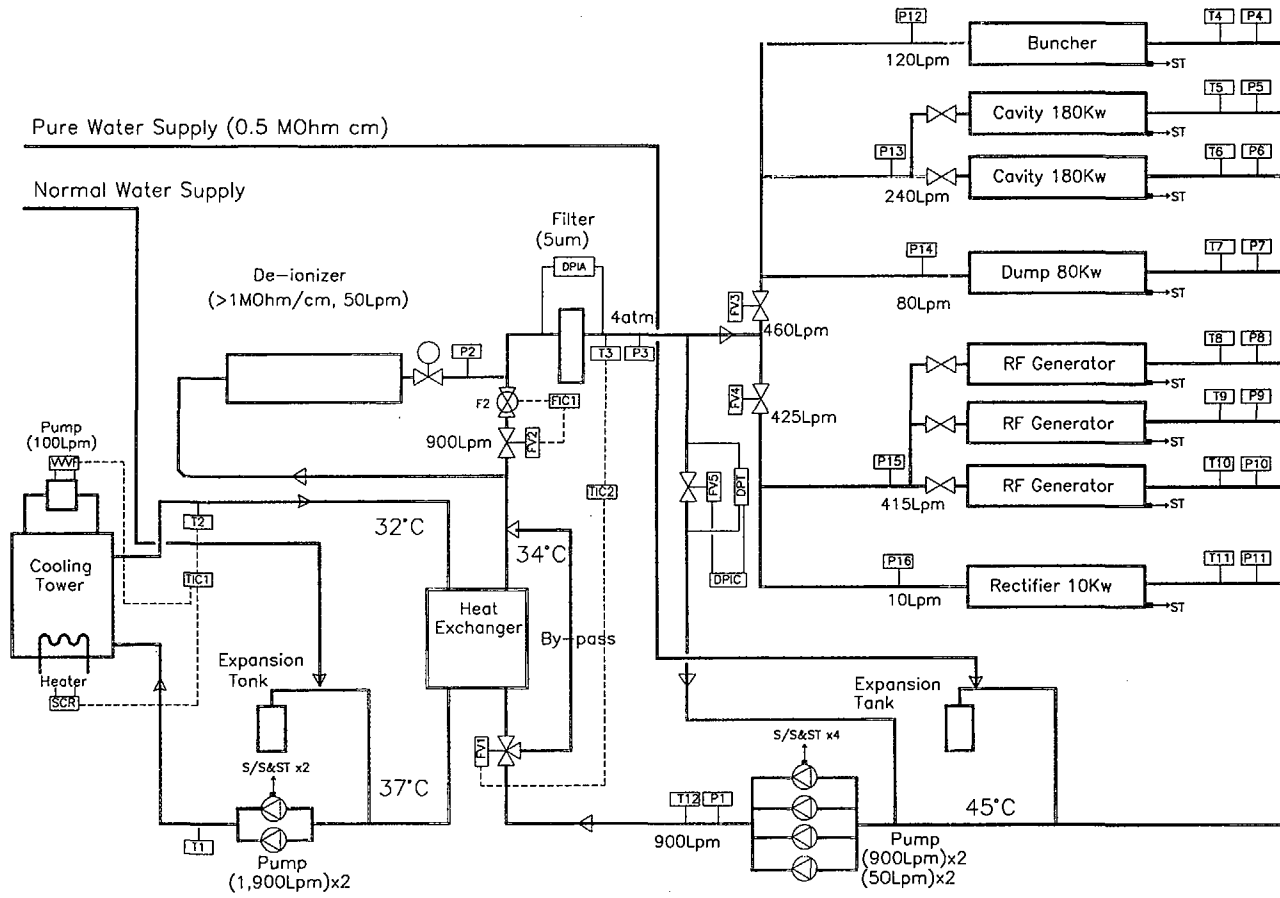
Figure 2.2.9 Schematic diagram of the cooling water system.

2.2.4 Conventional Utilities

Most of the conventional utilities for the AQBS project, such as, shielded building, electricity, cooling water system, air cooling system, and air ventilation system, have already been constructed. Figure 2.2.7 shows a photograph of the Engineering Research Building in which the rooms for the AQBS project are located. A 500 m^2 accelerator hall with 1.5-m concrete shielding is located on the basement floor of the building, and the other rooms for RF generators, electricity, and control system are located on the first floor.

The existing electrical power system, which was originally prepared for normal conducting version of a main accelerator has total power of 5.5 MVA. It is quite enough for the operation of the superconducting accelerator, the undulator, the power supplies of the beamline magnets, and the other user facilities. The voltage of the primary line of the transformer is 6.6 kV and the secondary line is divided into two parts, 380 V (2.5 MVA) and 220 V (3 MVA). The local distribution panels are located in the accelerator hall and upper floor for the RF generator, high voltage power supply, and controllers.

The tetrodes for the superconducting accelerator must be cooled down using deionized water. Approximately 300 lpm of cooling water is needed for this cooling. Two RS compressors of the cryogenic system require cooling water of 100 lpm at 25 °C. The existing cooling water system for the injector has a capacity of 1,000 lpm. With minor modifications (upgrade of pump capacity), it is possible to cool the whole accelerator system. The specific resistance of the water is more than 1 MΩ·cm and the oxygen content inside of the water keeps less than 2 mg/l using a special purifier system. The temperature of the cooling system is kept constant within ±1 °C. A photograph and a schematic diagram of the cooling water system are shown in Figure 2.2.8 and 2.2.9 respectively.

2.2.5 Future plan of the AQBS project

During the first phase of the AQBS project (1997-1999), most of the conventional utilities for the accelerator system (shielded building, electrical power system, water cooling system, and so on) were constructed. A high-average-current 2 MeV injector was developed. The injector opeartes routinely and all the parameters of the electron beam has been measured. An irradiation port of the 2 MeV electron beam is now being constructed according to the request of users.

The second phase of the project has already started at the end of 1999, and will end on December 2002. In the second phase, the development of main accelerator system, the construction of an irradiation facility of medium-energy electron beam, and the

detail design of the IR FEL system and particle beam sources are main goals. The medium-energy electron beam will be delivered to users at the beginning of 2003.

The first half of the third phase (2003-2005) of the project will be devoted to the lasing of high-average-power infrared FEL, and to the construction of beamlines for the generation of neutrons and positrons. The second half of the third phase will be focused on the generation of a wide range of monochromatic X-rays, high-flux neutron beams, and monochromatic slow positron beams.

Recently, the free electron laser laboratory at KAERI has been selected as the "**National Research Laboratory**" in the field of free electron laser by the Ministry of Science and Technology of the Korean Government. The FEL laboratory at KAERI will play an important role in the development of FEL technologies in Korea.

References

[2.2.1] S.O. Cho, B.C. Lee, Y.U. Jeong, S.K. Kim, and J. Lee, "Transient Behavior of the Terminal Voltage in a Recirculating Electrostatic Accelerator for a Long-pulse Free-electron Laser", Rev. of Sci. Instrum., 67(10), 3491 (1996)

[2.2.2] B.C. Lee, S.K. Kim, Y.U. Jeong, S.O. Cho, and J. Lee, "First Lasing of the KAERI Millimeter-Wave Free Electron Laser", Nucl. Instr. and Meth. A, Vol.375, 28 (1996)

[2.2.3] S.K. Kim, Y.U. Jeong, S.O. Cho, B.C. Lee, and J. Lee, "2-D Simulation of the Waveguide Free Electron Laser with a Helical Undulator", Nucl. Instr. and Meth. A, Vol.375, 219 (1996)

[2.2.4] S.O. Cho, Y.U. Jeong, B.C. Lee, S.K. Kim, B.H. Cha, J. Lee, and K.H. Chung, "Investigation of Electron Beam Transport in a Helical Undulator", Nucl. Instr. and Meth. A, Vol.375, ABS9 (1996)

[2.2.5] B.C. Lee, Y.U. Jeong, S.O. Cho, and J. Lee, "A Compact Far Infrared Free Electron Laser", Nucl. Instr. and Meth. in Phys. Research A, Vol.405, 195 (1998)

[2.2.6] S.O. Cho, S.K. Kim, Y.U. Jeong, B.C. Lee, B.H. Cha, J. Lee, G. Kazakevitch, and I. Spassovsky, "Time-resolved Measurement of Electron Beam Emittance and Energy Spread with Optical Transition Radiation", Nucl. Instr. and Meth. in Phys. Research A, Vol.407, 359 (1998)

[2.2.7] Y.U. Jeong, B.C. Lee, S.K. Kim, S.O. Cho, J. Lee, B.H. Cha, P.D. Vobly, Y.M. Kolokolnikov, S.F. Mihaylov, and G.N. Kulipanov, "Short-period

Equipotential-Bus Undulator for a Far Infrared Free-electron Laser", Nucl. Instr. and Meth. in Phys. Research A, Vol.407, 396 (1998)

[2.2.8]   J. Lee, Y.U. Jeong, S.O. Cho, S.K. Kim, B.C. Lee, B.H. Cha, G. Kazakevich, I. Spassovsky, P. Vobly, and G. Kulpanov, "Design and Construction of a Far-infrared Free-Electron Laser Driven by Microtron", Nucl. Instr. and Meth. in Phys. Research A, Vol.407, 161 (1998)

[2.2.9]   Y.U. Jeong, B.C. Lee, S.O. Cho, S.K. Kim, and J. Lee, "Investigation of Optical Resonator in a Far-infrared Free-Electron Laser Driven by an 8-MeV Microtron", to be published in Nucl. Instr. and Meth. in Phys. Research A, (1999)

[2.2.10] Y. Avlasov, *et al.*, "Control System for a Far-Infrared Free Electron Laser", to be published in Nucl. Instr. and Meth. in Phys. Research A, (1999)

[2.2.11] B.C. Lee, S.O. Cho, Y.U. Jeong, S.K. Kim, and J. Lee, "High Average Current 2-MeV Electron Accelerator for High-Power Free-Electron Lasers", Nucl. Instr. and Meth. in Phys. Research A, Vol 429, p.352-357 (1999)

[2.2.12] S.O. Cho, B.C. Lee, Y.U. Jeong, S.K.Kim, B.H. Cha, and J. Lee, "Measurement of Timing Jitter in a Train of Electron Pulses Using Wakefield Analysis", in Rev. of Sci. Instrum., Vol. 71, pp. 61-65, (2000)

3. Accelerator System

3.1 Introduction

At the beginning of the AQBS project, the 100 MeV accelerator system was designed on the basis of 180 MHz normal conducting RF cavities, which had been developed by the Budker Institute of Nuclear Physics, Russia. The 2 MeV injector, which was installed at KAERI in 1998, is based on the original design of the AQBS project. Figure 3.1.1 shows a schematic diagram of the 100 MeV accelerator based on the 180 MHz RF cavities.

With the existing 2 MeV injector, we estimated the costs of the main accelerator system in two different kinds of accelerating cavities: one is for the 180 MHz normal conducting (NC) cavity and the other is for the 352 MHz superconducting (SC) cavity. It was found that the SC accelerator system gives us benefits (in the sense of cost) compared to the NC accelerator system. Because of low acceleration gradient (i.e., 1 MeV/m) of NC RF cavity, more RF cavities and more recirculation turns are needed to obtain a high energy electron beam in the NC accelerator system. The comparision between the NC version and the SC version is listed in Table 3.1.1. Therefore, the beam line of the NC accelerator system becomes more complicate and expensive than that of the SC accelerator system.

Table 3.1.1 Comparison between the NC version and the SC version
for the 100 MeV accelerator system.

	NC accelerator	SC accelerator
Resonance frequency	180.3 MHz	352 MHz
Q value	42,500	3.4 × 109 @ 6 MV/m, 4.5 K
Acceleration gradient	2 MV/m	6 MV/m
# of cavities	16	4 cell × 4 cavities
Energy gain per turn	12 MeV	32 MeV
# of recirculation turns	8	3

The normal conducting accelerator, however, has an advantage: it can accelerate electron beams with higher average current. But its cost is too high and the requirement
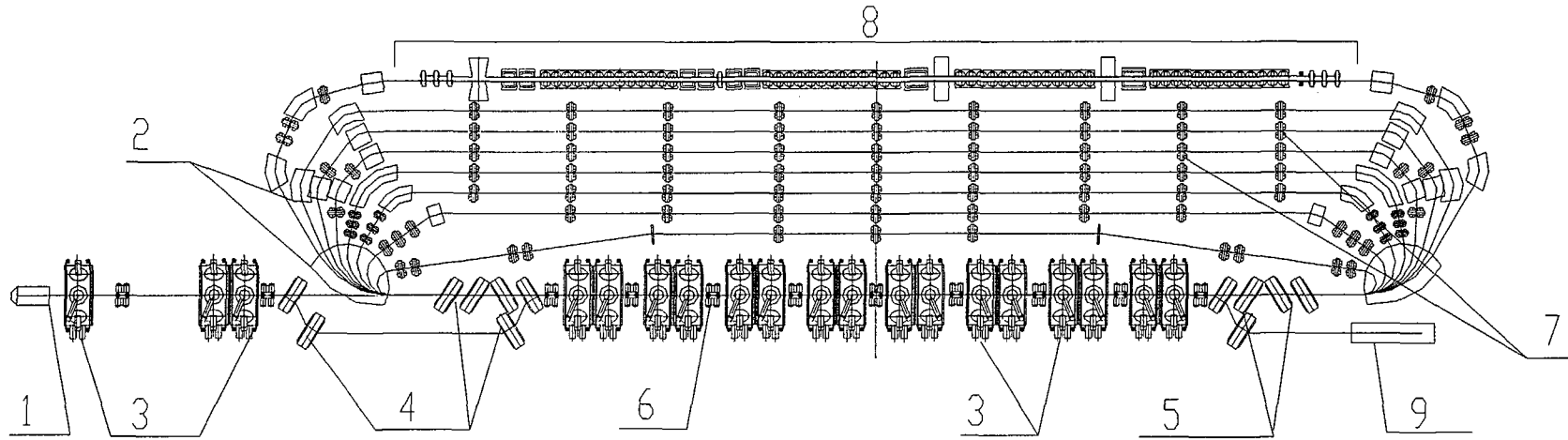
Figure 3.1.1 Schematic diagram of the 100 MeV electron accelerator based on 180 MHz normal conducting RF cavities. (1 - electron gun; 2 - bending magnets; 3 - RF resonators; 4,5 - injection and outcoupling magnets; 6 - focusing solenoids; 7 -straightsections with the quadrupole lenses; 8 - FEL magnetic system; 9 - beam dump).

2 MeV Injector

Main Accelerator

Dump

Target

Particle Beam
(e-, e+, n)

Photon Beam
(FEL, X-ray)

MIR or FIR FEL

Undulator-I

Optical cavity

Photon Beam
(IR FEL, X-ray, γ-ray)

Undulator-II

Photon Beam
IR FEL

27.25 m

$\textcircled{\textbf{H}}$ Quadrupole	$\textcircled{\text{B}}$ Bending magnet	$\blacksquare$ Bending magnet	$\textbf{K}$ Cavity mirror
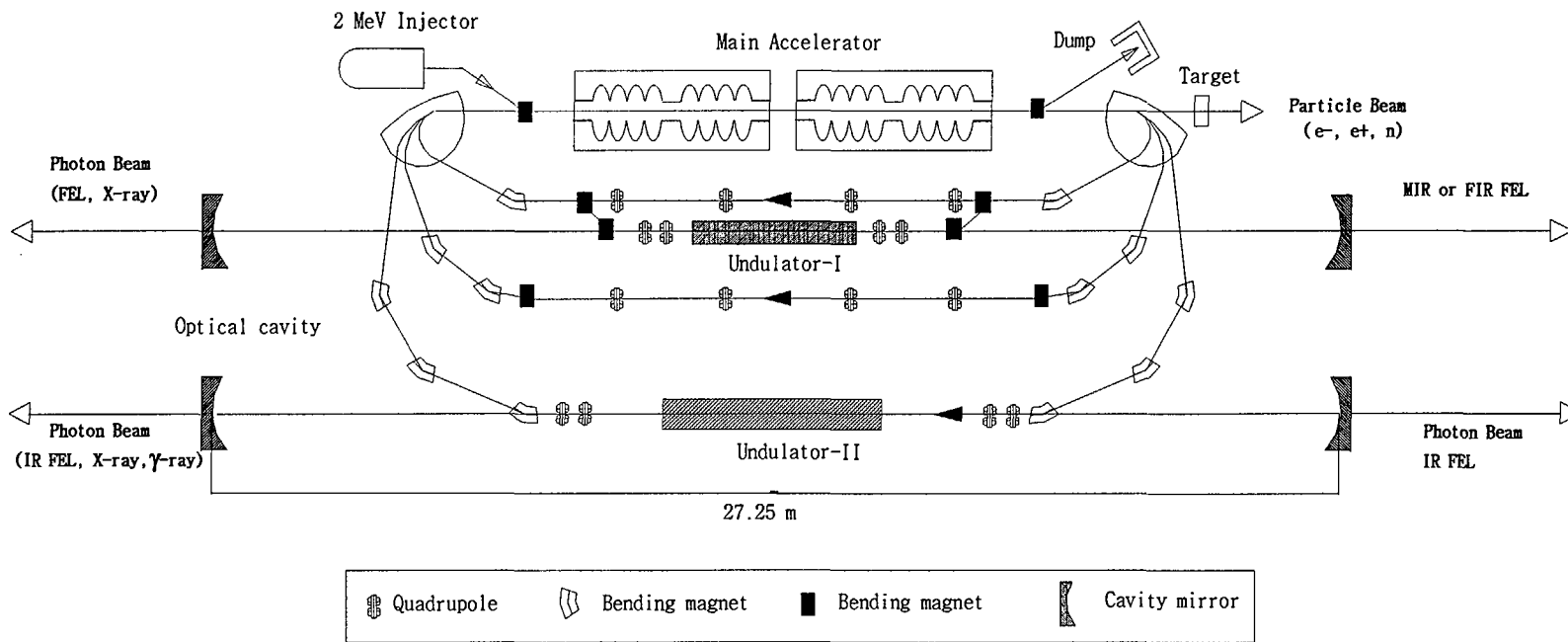
Figure 3.1.2 Schematic layout of the 100 MeV electron accelerator based on 352 MHz superconducting RF cavities

level of average current can be also obtained by using the superconducting accelerator. In addition, the rapid progress in the development of superconducting accelerator technology may enable us accelerate electron beams with higher current in future.

The usage of 352-MHz SPS SC cavities, after dismantling of LEP, will allow us to reduce the cost, the risk, and the time-scale of the AQBS project. Redesign of the accelerator system based on the SPS SC accelerator modules is going on at KAERI. Figure 3.1.2 shows a schematic diagram of the 100 MeV accelerator based on the SPS SC accelerator modules.

The electron accelerator will operate in two different modes: one is a "beam extraction mode" for particle beams and the other is a "energy recovery mode" for photon beams. The beam extraction mode is to extract an electron beam from the accelerator and transport to the experimental area. The electron beam is then irradiated on targets in order to generate neutrons and/or positrons or directly on various materials for the improvement of material properties. The parameters of the electron beam in this operation mode are as follow:

- Energy: 10 ~ 100 MeV (= 33 MeV/pass × 3 passes)
- Average beam power: max. 100 kW (= 25 kW/cavity × 4 cavities)
- Average current at targets: 1 mA (@ 100 MeV), 10 mA (@ 10 MeV)

The energy recovery mode is for the production of photon beams, such as, FELs, x-rays, and γ-rays. After interaction with optical fields under periodic magnetic fields, the 'spent' electrons re-enter the RF cavities at "deceleration phase' to convert their energy into the energy of RF fields. These electron beams are decelerated down to ~ 2MeV and dumped. The parameters of the electron beam in this operation mode are as follow:

- Energy: 20 ~ 100 MeV (= 33 MeV/pass × 3 passes)
- Average beam power: max. 1,000 kW
- Average current: 10 mA

The main advantage of this operation mode is to be free from high radiation hazard. The energy recovery system allows us to reduce the dumped power below 20 kW, while discharge of 1,000 kW electron beams to the dump leads to extremely high radiation hazard. In addition, a 2 MeV electron beam in the dump does not produce neutrons and low-energy γ-rays radiated by a 2 MeV dumped electron beam is easily absorbed by a relatively simple shielding blocks.

The consumption of RF power differs quite a lot in two operation modes. In the beam extraction mode, RF power of ~ 105 kW is needed, while, in the recirculation mode (energy recovery mode), only ~ 15 kW is needed.

Buncher Cavity

Acceleration Cavity

Electron Gun

Bending
Magnet

Dump   Kicker Magnet
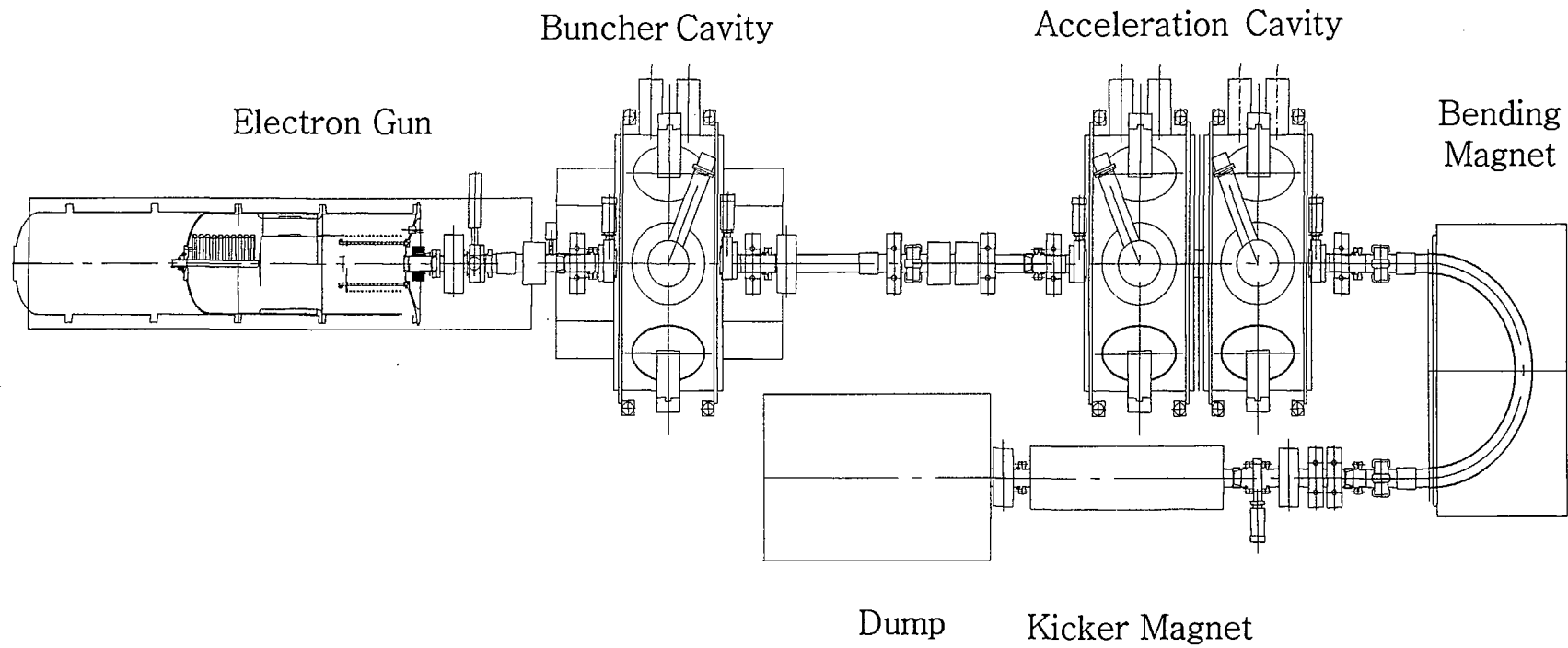
Figure 3.2.1 Layout of the injector system.
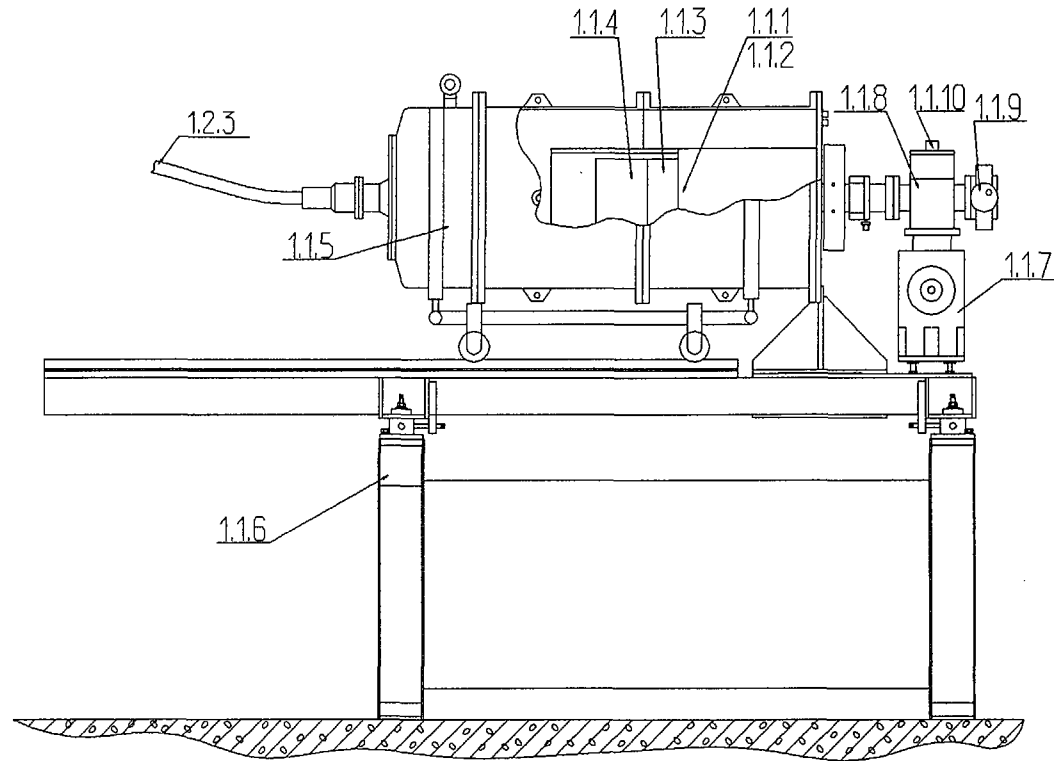
Figure 3.2.2 Layout of the electron gun. (1.1.1: cathode-grid unit; 1.1.2: accelerating tube; 1.1.3: modulator; 1.1.4: P.S. for modulator; 1.1.5: Housing; 1.1.6: Base; 1.1.7: Vacuum pump with power supply; 1.1.8: Angular gate; 1.1.9: Straight-flight gate; 1.1.10: Vacuum gauge)

3.2 Injector

The injector has been developed to supply high current electron beams for the main accelerating system. The layout of the injector system is shown in Figure 3.2.1. The main parameters of the injector are as follows:

- Electron energy (kinetic): 1.5 MeV
- Current

peak	: 6 A
average	: 45 mA

- Emittance   : 40π mm mrad
- Repetition rate   : 0 – 22.5 MHz
- Pulse duration   : 350 ps
- Operation mode   : CW/single pulse

3.2.1 Electron gun

The layout of the electron gun is shown in Figure 3.2.2. The electron gun is comprised of a cathode-grid unit, a static linear accelerating tube, a 300 kV power supply with control electronics, a power supply for the high-voltage part of the gun with an isolation transformer, and control electronics with optical signal transmission to and from the high-voltage part. The cathode-grid unit is manipulated by the controlled pulser and the static linear accelerating tube is placed in the high-pressure vacuum vessel with SF_6 gas insulation. The followings are parameters of the electron beam from the gun.

- Electron energy (kinetic) : 300 keV
- Current

peak	: 1.25 A
average	: 45 mA

- Emittance   : 160π mm mrad
- Repetition rate   : 0 – 22.5 MHz
- Pulse duration   : 1.6 ns
- Operation mode   : CW/single pulse

A cathode-grid unit is a source of thermal electrons and consists of a BaO:CaO:MgO cathode and two control grids. An accelerating tube is designed for focusing and accelerating electron beams. A system of focusing electrodes is located

inside the vacuum part of the accelerating tube and outside the gas part there is a high-voltage divider to maintain a uniform distribution of voltage along the whole length of the accelerating tube. In addition there are spark gaps on the outside electrodes for protecting the accelerating tube from breakdowns.

A modulator is used for generating nanosecond pulses of electron beams. It consists of a printed-circuit-board with ratio parts. The board is placed in the radiator. The parameters of the modulator are as follows:

- Output voltage: 150 V
- Repetition rate: 0 - 22.5 MHz (50 Ω)
- Pulse duration: ≤ 1.6 ns

A power supply for the modulator is designed to feed the shaper and the cathode-grid unit of the electron gun via computer control through a CAMAC crate. It consists of seven printed-circuit boards, located in the basic board. This device provides the following input voltages.

Power supplies in the cathode-grid unit

For a cathode filament (floating)	Voltage	(0.5 ÷ 8.5) V
	Current	4 A
	Instability	± 1%
For a cathode bias	Voltage	+(30 ÷ 60) V
	Current	- 0.1 A
	Instability	± 1%
For a grid 2	Voltage	+(150 ÷ 350) V
	Current	0.08 A
	Instability	± 1%

Power supplies for the shaper

For IC	Voltage	+9 V
	Current	0.5 A
	Instability	± 1%
For a positive voltage	Voltage	+(20 ~ 50) V
	Current	0.7 A
	Instability	± 1%

For a negative voltage	Voltage	-(20 ~ 50) V
	Current	0.8 A
	Instability	± 1%

High voltage power supply of the electron gun is capable of generating maximum power of 15 kW with output voltage of 300 kV. SF_6 gas is used for an insulating medium of the pressured tank for the high voltage rectifier.

3.2.2 RF cavity

The injector has a bunching cavity and two pre-accelerating cavities. Design of a RF cavity is shown in Figure 3.2.3. The cavity has a conical shape in side view. It is good for mechanical rigidity and electrical characteristics of the cavity. The fundamental cavity mode is of an TE_{010}-like type. It has longitudinal electric field with angular symmetry. Main characteristics of the cavity are summarized in Table 3.2.1.

The bunching cavity is used for reducing the pulse duration and increasing the peak current of the electron bunches generated from the gun. It has just same geometry as the accelerating cavity. The difference compared with the accelerating cavities is only that the cavity is not combined in a pair and the necessary RF-voltage is less by an order of one (the power is less by an order of two). Therefore this cavity can have lower values of Q-factor, voltage limit, and so on. The estimated RF voltage in the cavity is 110 kV. The phase of RF power is chosen so that the energy of electrons should be decreased by an amount of 30 kV after passing the cavity. The power lost by electrons is comparable to that fed into the cavity. Due to this phenomenon the control system should be designed very carefully in order to maintain the phase and the amplitude of RF voltage in the cavity.

The accelerating cavities are for increasing the beam energy, while avoiding the slope of the longitudinal phase portrait of a bunch made by the bunching cavity, and are necessary for the bunching process. To reach the final energy of a bunch to 1.5 MeV, the voltage on each cavity should be ~ 700 kV taking into account of margins for the flight factor and the non-zero phase of a pass. As the normalized emittance grows proportionally to γ^{-2} (the relativistic factor), one gains ~ 6 if the energy of electrons is increased to 1.5 MeV and so does the longitudinal phase volume. The bunching process is effective only during a pass from the bunching cavity to the first accelerating one. Hence there are no direct restrictions on the size and position of the injector. Additionally, independent control over energy, bunch length, and slope in the longitudinal phase space of the beam is possible.
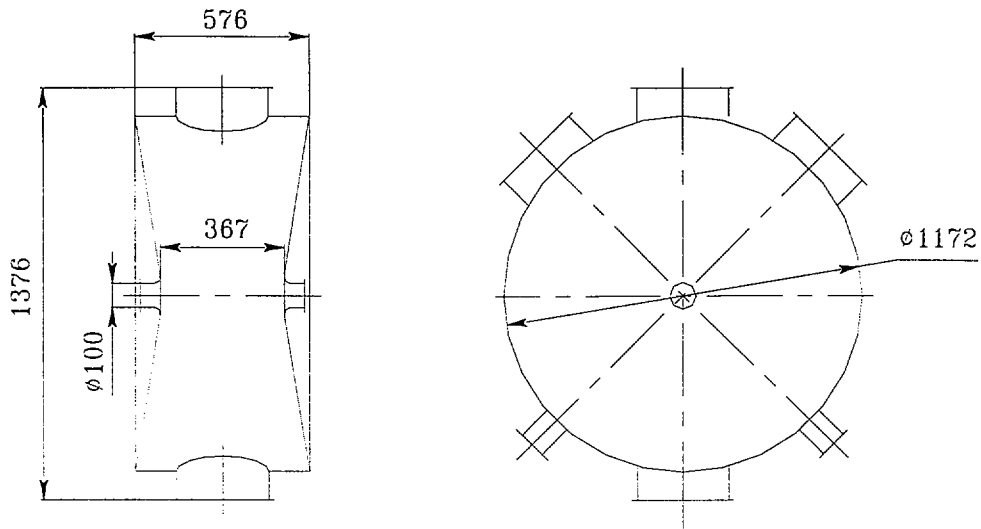
Figure 3.2.3 Schematics of the RF cavity
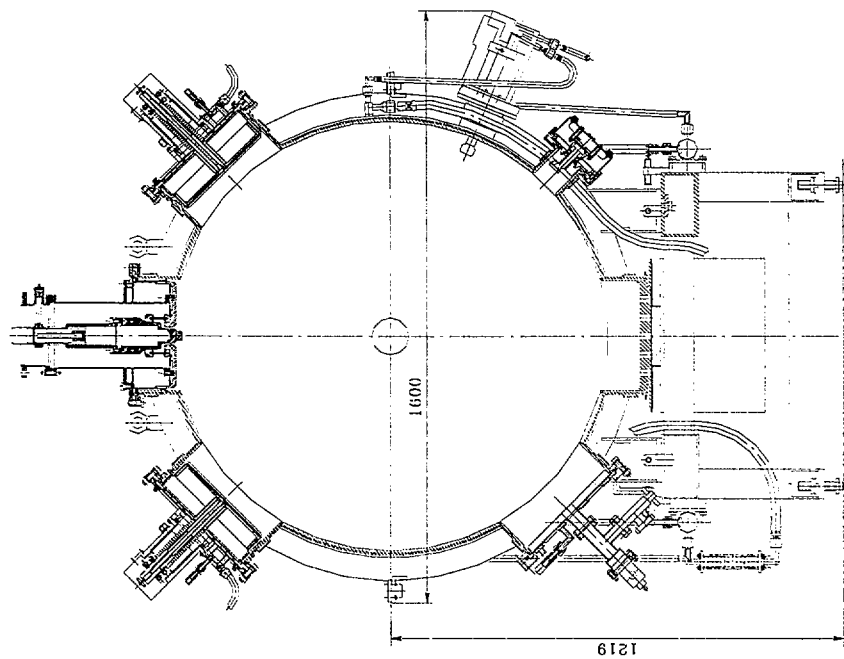
Figure 3.2.4 Insertion units of the RF cavity.

Cavities have copper clad stainless steel walls. They have low RF losses due to low RF resistance of copper. High thermal conductivity and large thickness (8 mm) of the copper exclude any excessive high temperature rise at the cavity surface. The stainless steel (7 mm thick) provides mechanical strength and prohibits corrosion. All cavity parts are joined to each other by TIG welding.

Different units are assembled to cavity flanges. One is a main coupler and the other is a sampling loop. The main coupler has a coaxial design. A cylindrical ceramic RF window is incorporated in it. The coaxial input line has a wave impedance of 75 Ω and the diameters of its outer and inner conductors are 160 mm and 45 mm, respectively. The sampling loop provides electrical signals, the amplitude and the phase of which are proportional to the amplitude and phase of the cavity voltage.

Table 3.2.1 Parameters of the RF cavity.

Accelerating voltage	40-1000 kV
Q value	42,500
R/Q value	212 Ω
Shunt impedance	9.0 M Ω
Resonance frequency	180.4 MHz
Tuning range of cavity frequency	360 kHz
Tuning rate	5 kHz/s
Power loss at V = 1000 kV	110 kW

Two main tuners are used basically for tuning the fundamental mode. Two additional HOM tuners are installed for making corrections of frequencies of higher order modes of the cavity. Because under some unfavorable circumstances the higher order modes may cause beam instabilities.

High vacuum in the cavity (10^{-7}-10^{-8} Pa) is obtained by means of a pumping unit PVIG-630, which is a combination of a sputter ion pump and a gettering pump. But such a high vacuum can be achieved only after baking out the cavity up to temperature of 300-400 degrees Celsius after its assembling. It is possible to do by using tape heaters and thermal insulations, mounted on the outer cavity walls.

Walls of the cavity and its units are cooled by demineralized water. Special water channels are provided in the stainless steel parts of the cavity walls for this purpose.

Any contact of water with copper walls is excluded. The water distribution system is mounted under the cavity, inside its support frame.

The RF cavities have been successfully tested up to 1200 kV of the accelerating voltage. This voltage level was achieved after many hours of RF processing to suppress multipacting. Coaxial RF windows have been tested up to 170 kW in RF power level.

3.2.3 RF generator

RF generators are dedicated to excite one bunching and two accelerating cavities of the injector. The operation frequency of all the generators is 180 ± 3 MHz. The schematic diagram of the RF generator system is shown in Figure 3.2.5. In Figure 3.2.6, the layout of the RF generator system is illustrated.
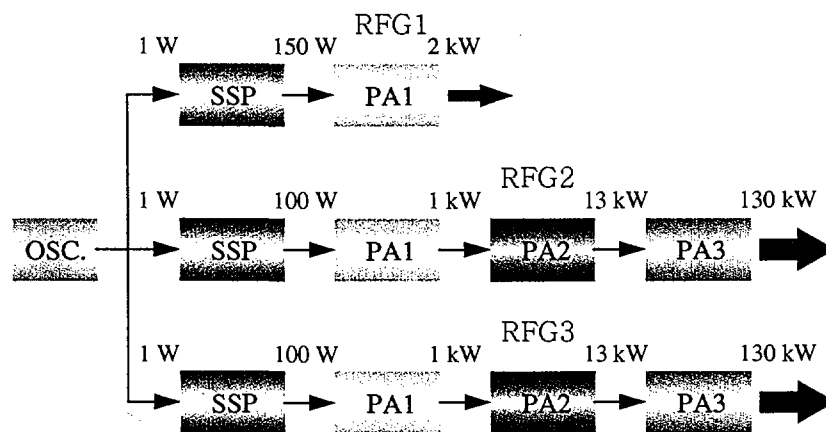
Figure 3.2.5 Schematic diagram of RF generator system. SSP is a solid-state power amplifier and PA1 and PA2 are power amplifiers based on tetrode typed GU-92A. PA3 is a final power amplifier for accelerating cavity with a tetrode GU-101A

Two RF generators that excite the accelerating cavities make up 3-stage power amplifiers. The stages are linked with each other by coaxial lines. The input power of the first stages of the generators is 100 W. The output power of each of the generators is 130 kW. The total power of the two generators is 260 kW. The powerful RF generators are linked with the cavities by coaxial cables. The impedance of a cable is 75 Ω and the outer and inner diameters of cable are 160 mm and 45 mm, respectively. To measure the return coefficient of RF cavity at the feeders there are mounted directional dividers

with a transition attenuation of 50 dB. Design of the feeders provides the flexibility in initial setting of the coaxial cable length that complies with the operation conditions of the generator in the injector.
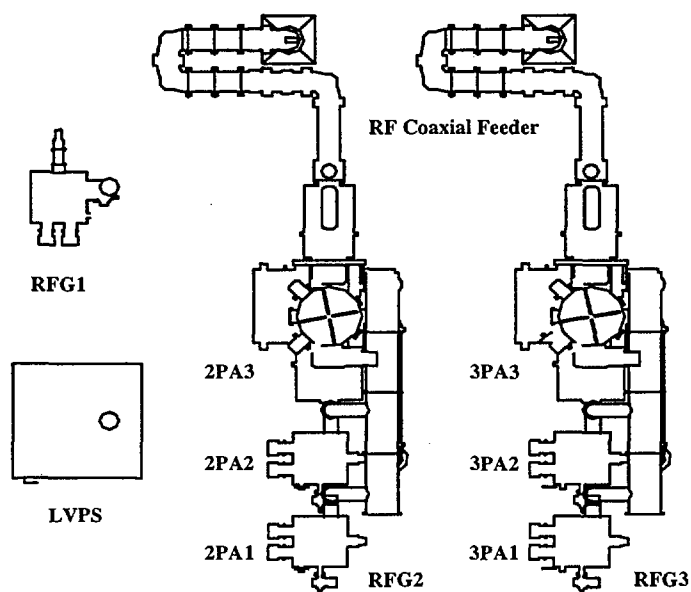
Figure 3.2.6 Layout of the RF generator system. LVPS is a low voltage power supply for RF generators.

The generator that excites the bunching cavity makes up a one-stage power amplifier. Its output power of 2 kW is determined by a value of voltage across the bunching cavity. Design of the power amplifier is similar to that of the preamplification stages of the three-stage generator. The RF generator is linked with the bunching cavity by a flexible coaxial cable in polyethylene insulation. The impedance of the cable is 50 Ω. The outer diameter of the cable is 50 mm. The RF generator system is located on a room upper than the accelerator hall and the connection between them is expressed in Figure 3.2.7.

The output and pre-amplification stages of the generator were made using GU-101A tetrodes including water cooling. The output power of the pre-amplification is 15 kW. The parameters of the RF-sections of the generators are summarized as follows:
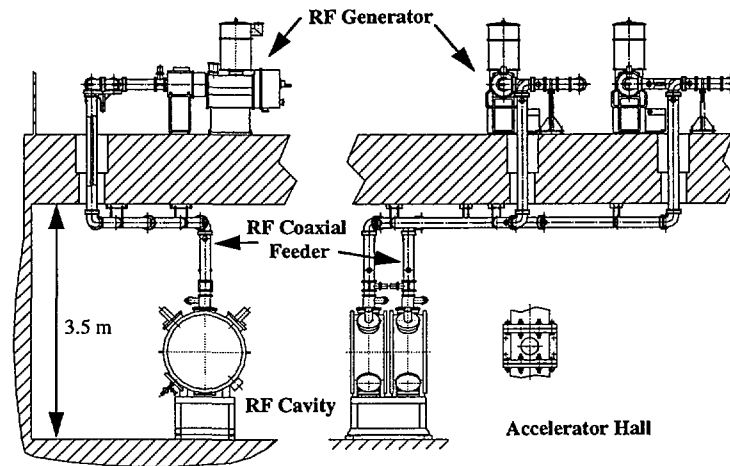
Figure 3.2.7 Cross sectional view of the combination between the RF generators and RF cavities.

1. Generator for bunching system
   - Frequency   :   180 MHz
   - Output power   :   1.7 kW
   - Anode voltage   :   8 kV
   - Anode current   :   1 A

2. Generator for accelerating system
   - Frequency   :   180 MHz
   - Output power   :   260 kW
   - Anode voltage   :   8 kV
   - Anode current   :   56 A

3. Anode power supply
   - Output nominal voltage :   8 kV
   - Output current   :   80 A

All the amplifiers are designed using a scheme with common grids and are energized from the power sources located in separate racks. The low-voltage racks contain power sources for filament, bias voltage, and screen grids. Operating voltage of

screen grids of all tetrods is +950 V. Bias voltage of the control grids of the GU-101A tubes is -200 V and of the GU-92A tubes is -150 V. An anode rectifier with a fast anode protection system allows one to feed variable voltages from +4 to +8 kV into tetrodes of the generator with current up to 80 A. The anode rectifier is placed in 8 racks. All tetrodes of the generator are cooled with deionized water. Besides, forced air is used for cooling of the RF stages.

3.2.4 Upgrades

Upgrade of the injector system is focused on matching of the RF frequencies between the injector and main accelerating system. The RF frequency of the SC cavity is 352 MHz, which is slightly lower than the double of RF frequency of the injector system. Modification of the RF generator system and RF cavities is now under consideration for operating them at the RF frequency of 176 MHz.

Another program for changing the thermionic gun to a photocathode gun has been studied. We have developed a photocathode with high efficiency based on the semiconductor materials of Cs_2Te. The fabrication process and the performance of the photocathode have been studied. Design of the photocathode gun is underway.

3.3 Superconducting RF Cavity

3.3.1 Specification of the RF Cavity

Superconducting cavities are used for an accelerator to get high accelerating gradient with low wall losses. The conceptual design using two 352 MHz SPS SC cavities is underway. The accelerator has two cryostats and each cryostat contains two 4-cell cavities. The specification of the cavity is shown in Table 3.3.1. Figure 3.3.1 shows overview of one of the CERN LEP cavities with cryostat [3.3.1]. Each cavity (which is made of OFHC copper with thin Nb coating) is equipped with a power coupler, which can deliver 150 kW CW, and four higher order mode (HOM) couplers. The geometry of cavities and cryostats is unchanged except HOM couplers.

The resonant frequency of the cavity can be tuned by controlling the cavity length. Three nickel bars are connected to the cavity beam pipes. The cavity length is adjusted by changing the length of the nickel bars. The length of the nickel bars, which depends on its temperature, is controlled by electrical heaters and cold He gas. Furthermore, the magnetorestrictive behavior of nickel can control the cavity length for fast frequency variation during operations.
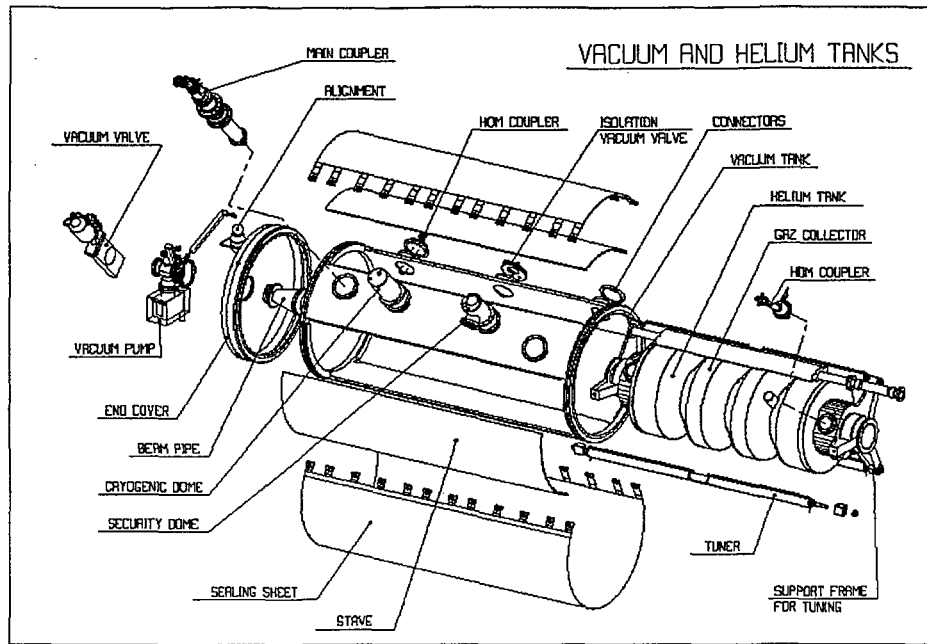
Figure 3.3.1 Overview of the cavity and the cryostat

Table 3.3.1 Basic parameters of the superconducting cavities

Fundamental resonant frequency	352 MHz
Cavity material	Nb-coated copper
Number of cell	4-cell 1 cavity
Q_0	3.4×10^9 at 6 MV/m, 4.5 K
R/Q	500
Frequency tuning range	50 kHz (maximum)
Active length of the cavity	1.7 m

3.3.2 Input couplers

The accelerator is operated in two different operation modes: beam extraction mode and recirculation mode. Both operation modes have the same cavity voltage of 8.3 MV but have different beam current. Since the beam current is 1 mA for the extraction mode, more than 100 kW (= 100 MeV×1 mA) should be transferred to the cavity. In the recirculation mode, an electron bunch of 10 mA current is accelerated

from 2 MeV to 100 MeV and then decelerated down to 2 MeV after generating FEL. Most of the RF power to accelerate the beam is recovered while the beam is decelerated. As a result, only about 5 kW will be required for the recirculation mode to compensate cavity wall loss and the FEL output loss.

The RF power is transferred to each cavity through input couplers attached to the cavities. In order to make the reflection power zero for the beam loaded cavity, which means transfer of all power from the RF source to cavity, the coupling coefficient β of the coupler must satisfy the following relation:

$$\beta = 1 + P_b / P_w = P_0 / P_w, \tag{3.3.1}$$

where P_b is the beam power, P_0 is the incident power to the cavity, and P_w is the wall loss power. The cavity voltage is expressed by the coupling coefficient:

$$V_a = (P_w Z)^{1/2} = (P_0 / \beta \ Z). \tag{3.3.2}$$

For the accelerator, V_a should be the same in the two different operation modes and thus

$$P_w = P_0 / \beta = \text{constant}. \tag{3.3.3}$$

Here, two different modes require a quite different value of P_0 ($= P_b + P_w$) because of different beam power and thus β should be adjusted according to Equation 3.3.1.

In order to satisfy both the cavity voltage and the zero reflected power for the two different operation modes, β should be changed appropriately. Thus, the input couplers of the cavities must be designed to have an adjustable coupling ratio. The variable couplers make the acceleration operation be more flexible.

3.3.3 HOM couplers

In a recirculating linac, multipass regenerative beam break-up caused by the HOMs is a serious factor limiting operating currents. Since the average beam current inside the cavity is 60 mA in the recirculation mode, the HOM couplers should be specially designed to reduce the beam instability. Intensive studies must be done to avoid the instability due to high order modes in the RF cavity. They couple the HOMs via a magnetic loop and transport the HOM power to the RF absorber installed outside the cryostat. The HOM couplers have rejection filter for fundamental mode of the cavity. We expect that at least two pairs of HOM couplers are needed for the AQBS system.

3.4 RF System

3.4.1 High power RF system

The maximum RF power required to accelerate the electron beams is 100 kW. However, due to RF losses in the waveguides, the reflected power from the cavity input coupler, and the redundancy, the RF system is designed to have the power of 200 kW at 352 MHz.

There are three kinds of commercially available RF power amplifier [3.4.1] that satisfies the requirement of the RF power: a tetrode, a diacrode, and a klystron. The specifications of these systems are shown in Table 3.4.1.

Table 3.4.1 Comparison of the RF amplifiers

Type	Power	Frequency	Number of pieces	Driver	Necessary electricity
Tetrode (TH 571B)	200 kW	350 – 370 MHz	4	2 tetrodes (TH 593)	11 kV 40 A
Diacrode	200 kW	350 – 370 MHz	1	1 tetrode (TH 561)	11 kV 35 A
Klystron (TH 2089)	1 MW	352 MHz	1	Solid-state amplifier (100 W)	100 kV 20 A

The tetrode (for example, Thomson TH 571B) has the maximum output power of 60 kW CW and 4 pieces of the tetrodes should be used for the cavities. Since each tetrode feeds RF power to each RF cavity though the waveguide, the phase and amplitude of RF power inside of the cavity can be controlled separately. In this system, circulators are not necessary, because the reflected power from the cavity does not damage the tetrode if the electrical length from the tetrode and the cavity is a half-integer of the RF wavelength.

The diacrode has the maximum output power of 170 kW and could be upgraded up to 200 kW. RF power generated from the diacrode is divided by directional couplers properly and then is distributed to each RF cavity. The phase of the RF voltage is controlled by changing the waveguide length between the diacrode and each cavity. Unlike a tetrode, a single diacrode can deliver the required RF power for the accelerator. It is the simplest and the most cost-effective.

The klystron TH 2089 was developed for LEP cavities. It was designed to have the output power of more than 1 MW. Thus it has lower efficiency (less than 45%) at 200 kW power level and requires high operating costs. Another possibility for using klystrons is to modify the existing klystron TH 2145, which has the output power of 200 kW at 368 MHz. However, this needs a new design for modifying the center frequency which results in increase of the cost.

The best choice of the high power RF amplifier is four-tetrode system. This system allows flexible accelerator operation because the phase and the amplitude of each cavity can be separately controlled. Furthermore, a circulator is not necessary while it is indispensable in both a diacrode system and a klystron system.

3.4.2 Low power RF system

Low power RF system controls the amplitude and phase of RF voltage inside the cavity and the resonant frequency of the cavity. It also protects the cavity and the RF system from fault conditions. The phase and the amplitude of the RF voltage can be fluctuated due to Lorentz force detuning, cryogenic pressure, mechanical oscillation of the cryostat, and so on. The fluctuations affect the beam circulating in the cavities and a tight allowance is needed for the recircualtion operation mode. In the Jefferson Lab, the requirements are $\pm 0.2°$ for phase stability and $\pm 2 \times 10^{-5}$ for amplitude stability [3.4.2].

The requirements on the phase and the amplitude stability are mainly determined by energy spread of the beam. The accelerator requires the energy spread less than 2.0×10^{-3}. This value comes from the beam quality requirements for both the FEL and the recirculation of the beam without losses. Actually, since the beam will get much larger energy spread after the FEL interaction in the undualtor, a special device for the energy compression is required. In this chapter, we consider the effect of the RF errors on the energy spread.

The amplitude variation changes the center energy of the bunch and is directly proportional to the offset energy. The relation between the phase error and the energy spread is given by

$$\sigma_E / E = \omega \sigma_z \Delta\varphi / c , \qquad (3.4.1)$$

where σ_E is rms beam energy spread, σ_z is bunch length. Here, the energy spread due to the bunch length is derived from

$$\sigma_E / E = \frac{1}{\sqrt{2}} \left(\frac{\omega \sigma_z}{c} \right)^2 , \qquad (3.4.2)$$

which gives the value of 9.6×10^{-4} for the electron beam with the bunch length of 5

mm. Considering the errors, the amplitude and the phase are correlated. Hence the amplitude stability should be less than 1.2×10^{-3} and the phase error, $\Delta \varphi$, should be within $1.8°$. More exact requirements for the stability of the phase and the amplitude will be obtained by computer simulations.

The schematic diagram of one RF control channel is shown in Figure 3.4.1. A fast - cavity feedback loop is used to stabilize the phase and the amplitude. A direct RF feedback of the RF frequency is implemented to reduce the beam-loading effects on the RF system and to improve the beam stability.
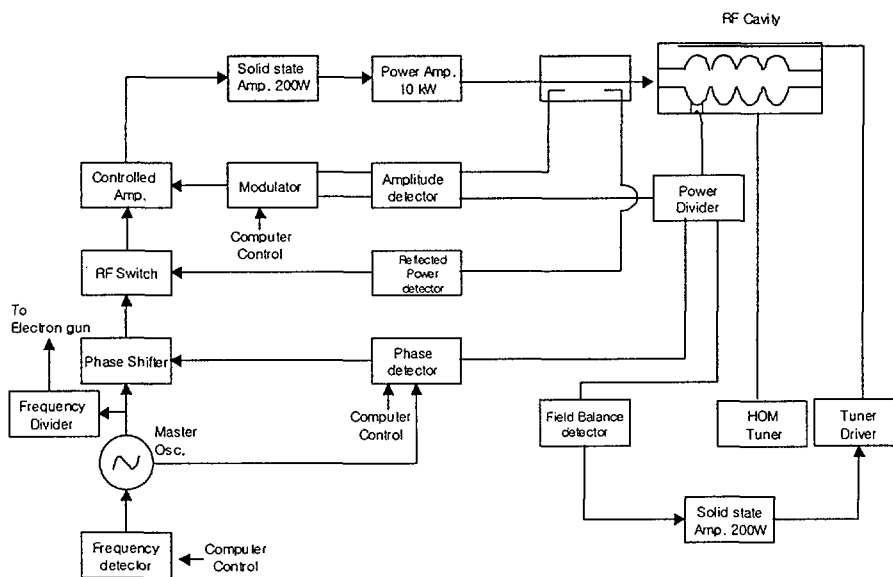
Figure 3.4.1 Schematic diagram of the RF control channel.

3.5 Cryogenic System

3.5.1 Cryogenic Load

The cryostats of the CERN SPS and LEP superconducting cavities have no thermal radiation shield and thus have large heat losses compared to those of TESLA, JAERI, ESS, and etc. For example, the TESLA cryostat has just 2 W static heat load although the operating temperature is 1.8 K. However, the conceptual design of the AQBS superconducting accelerator at KAERI is based on the specifications of the CERN SPS cavities, because of easy accessibility and low cost. Two cryostats will be installed in

the accelerator. There is no big difference in heat load on the cryostats between with and without thermal shield. Each cryostat has two cryogenic bathes with volume of about 200 liters. The heat load of total system is as follows.

a) Static Load
- Cryostat : 40 W/cryostat × 2 cryostats
- Transfer Line (40 m) : 40 W
- Dewar + Distribution Box: 20 W

b) Dynamic Load*: 70 W/cavity × 4 cavities = 280 W

- $^*E_a^2 \cdot L^2_{act}/(Q_0 \cdot R/Q)$

- L_{act}: 1.7 m
- Q_0: 3 x 10^9 at E_a = 6 MV/m
- R/Q: 500
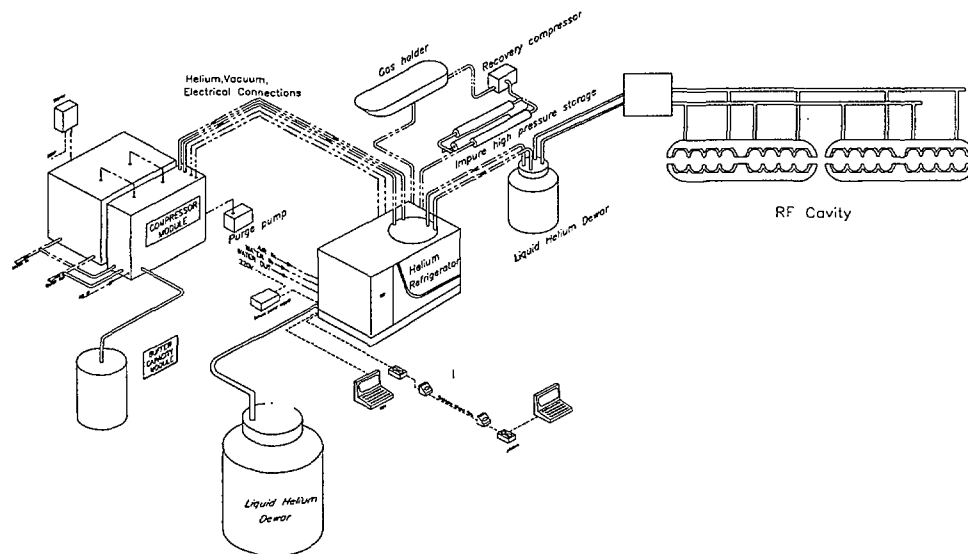
Figure 3.5.1 Schematic diagram of the cryogenic system.

3.5.2 Specifications of the cryogenic system

The cryogenic system will be composed of two cold boxes (PSI 1603 Helium liquefaction and refrigeration system) for each cryostat. The maximum heat capacity is 218 W at 4.5 K and the liquefaction rate is 70 liter/hour. It will be pre-cooled by liquid nitrogen. The pressure of liquid helium is 3 psi higher than the atmosphere. Each cold box has two sets of 100 kW rotary screw compressor. The specifications of cryogenic system are listed in Table 3.5.1 and the schematic diagram is shown in Figure 3.5.1. A distribution box distributes liquid helium from a 2,000 liter dewar to each of four cavity bathes. The inlet and outlet valves of each cryo-module control the level and pressure of the liquid helium inside the bathes. The cryogenic system will be operated automatically via PLC during normal operation at 4.5 K although it needs to be operated manually during cool-down from room temperature to 4.5 K.

Table 3.5.1 The specifications of the cryogenic system

Number of cold box	2
Temperature	4.5 K
Pressure	3 psi
Heat Capacity of each cold box	218 W at 4.5 K (with liquid nitrogen pre-cooling)
Liquefaction rate of each cold box	70 l/h
Dewar capacity	2,000 liter

3.5.3 Components of the cryogenic system

The components of the cryogenic system are as follows:

1) Helium liquefier and refrigerator module 1 set
- liquefaction rate: 70 l/h
- maximum heat capapcity: 218 W at 4.5 K with liquid nitrogen precooling and full flow of RS compressors
- automatic control with PLC
- automatic Joule-Thomson and return valve

2) Helium compressor module 2 sets
- rotary screw compressor with oil removal system
- suction pressure: 0.5 – 2 atm

- discharge pressure: 18 atm

3) Integral automatic purifier

4) Medium pressure helium gas storage tank

- Capacity: 16 m³

5) Liquid Helium Dewar

- Capacity: 1,000 liter
- Pressure indicator, relief and vent valves included
- Level meter: 4-20mA output signal
- Connectors : 3 connectors with 1/2" adapter

6) Cryogenic adsorber

- He Purity: > 99.9%

7) Coaxial Delivery Tube

- Heat load: < 1 W/m
- Horizontal length: 5 m
- Vertical length: 3 m

8) Accessories

- Test and trainingt
- Acoustical Enclosure for RS compressor
- Annunciator for RS compressor
- Installation Fitting Kit (Stainless Steel 304)
- Liquid Helium Transfer Line

3.6 Beam diagnostics

3.6.1 Beam current monitors

DC current monitor

The electron beam generated from the gun has the bunch length of 1.6 ns with a repetition rate up to 22.5 MHz. To avoid vacuum chamber damages due to loss of the high power electron beam, a special attention was paid to beam intensity monitoring. When a measured loss of electron beam current through the transport beam lines is above the threshold (or interlock level setting), the injection system will be interlocked. The schematic of DC current monitor is shown in Figure 3.6.1. DC monitor system, which is called Second Harmonic Detector [3.6.1], consists of parametric current transformer, wide band AC transformer, permalloy guards, and steel cover to remove

the returning wall current. The parametric current transformer consists of two permalloy cores with 100-turn windings and 100-turn common winding. First windings are used for excitation and as a second harmonic detector simultaneously while common winding is for compensation current. The AC transformer with a frequency band from DC up to 100 kHz consists of permalloy core, 100-turn compensation winding, and 400-turn AC feedback winding. The sensitivity is 10 mA/V. The monitoring systems are located after the gun and before the electron beam collector. The current loss is the difference of the currents between two points.
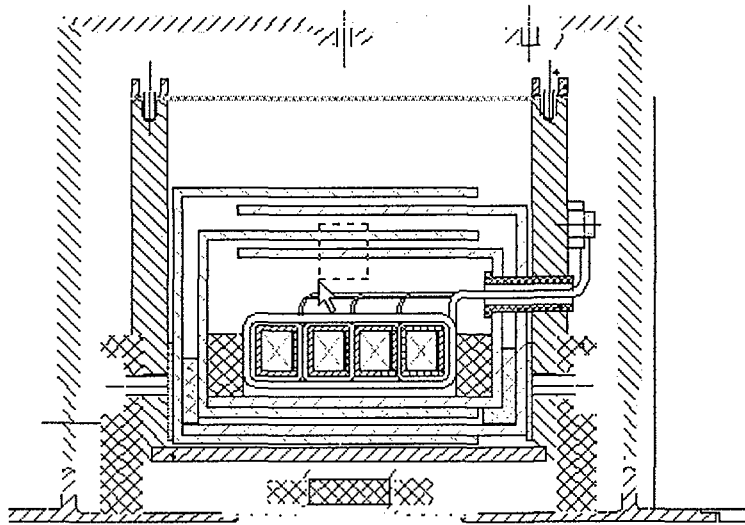
Figure 3.6.1. Schematic of DC current measurement system.

Wall current monitor

The wall current monitors, which are a system for measuring the image current, are already installed in three positions: after the gun, after the buncher cavity, and before the electron beam collector. After insulating the beam pipe with the ceramic ring, sixteen 50 Ω resisters are connected in parallel, as shown in Figure 3.6.2. The wall current can be measured by measuring the voltage of one of resisters using the oscilloscope. The peak current and time structure of electron beams can be measured with a time resolution of 100 ps and a sensitivity of 3.1 volt/ampere. In the 2 MeV injector at KAERI, the pulse width of electron beam from the gun is about 1.6 ns, while after the buncher cavity is about 300 ps, as shown in Figure 3.6.3.
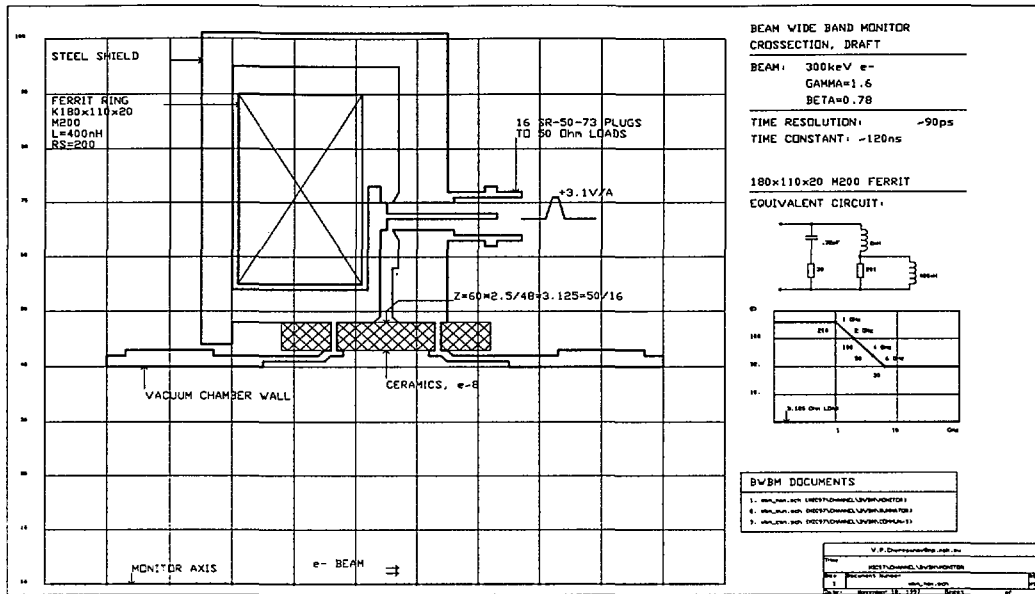
Figure 3.6.2. Schematic of Wall current measurement system.
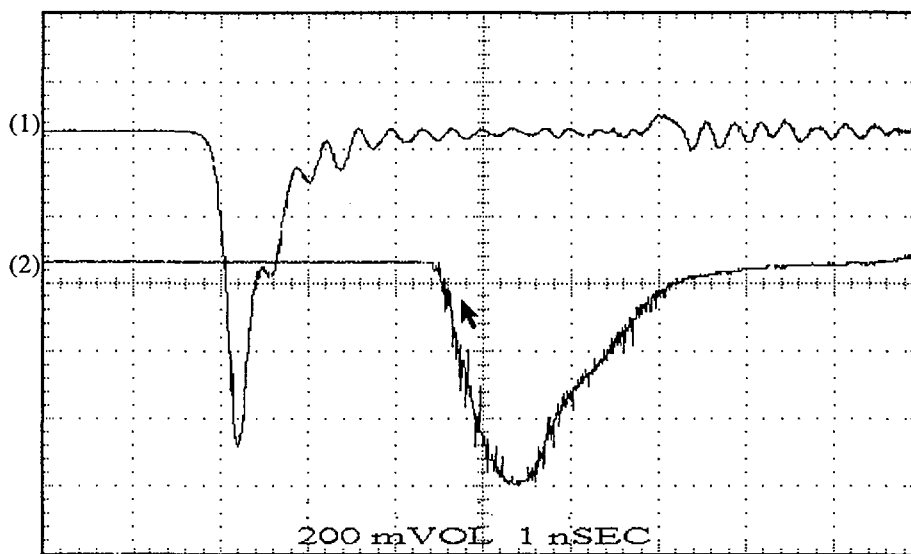
Figure 3.6.3. Temporal structure of the electron beams.

(1) electron beam after the buncher cavity

(2) electron beam from the electron gun

51
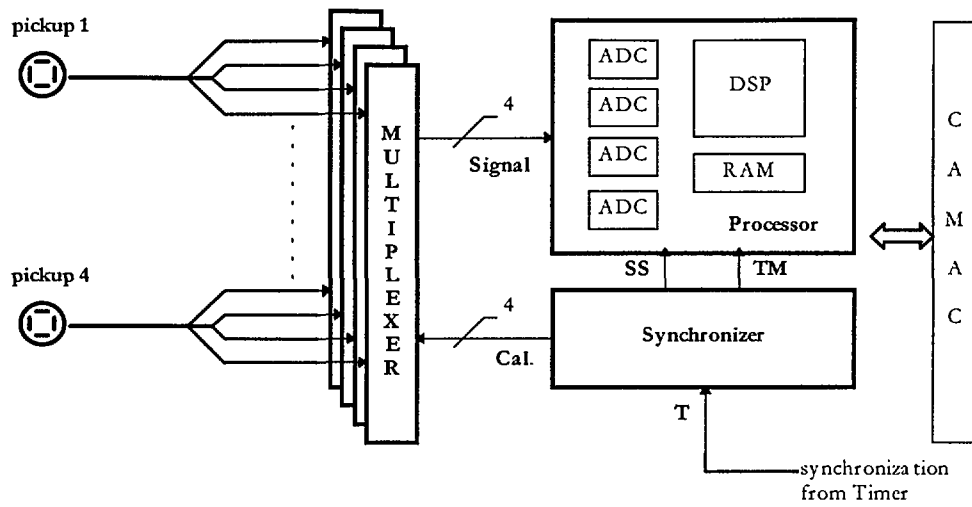
Figure 3.6.4 A block diagram of the BPM (Beam Position Measurement) system.
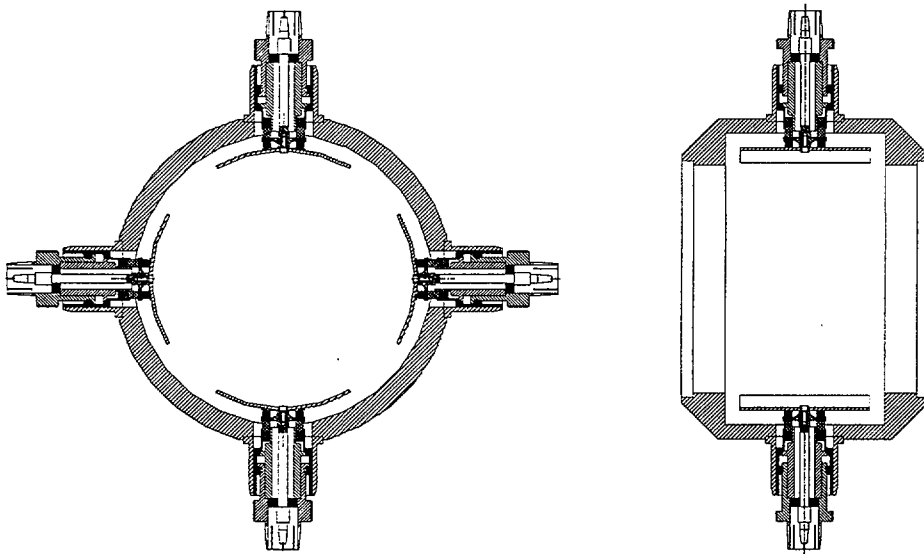
Figure 3.6.5 Schematics of the BPM (Beam Position Measurement) pick-up devices.

3.6.2 Beam Position Measurement (BPM) system

The BPM system allows measuring the electron (or positron) beam position in the beam lines. Four pickups are already installed in the 2 MeV injector system and operational. The measurement system consists of four electrostatic pickups, four Multiplexers, the Synchronizer, and the four-channel Signal Processor modules. The measurement system in the acceleration system including the recirculating beam lines will be the same as those in the injection system.

The block diagram of the BPM system and the pick-up device are illustrated in Figure 3.6.4 and 3.6.5. The main idea is based on the simultaneous measurements of signal amplitudes from the four electrodes of the pickup, followed by digital data processing to obtain the beam position.

The signals from the electrodes of pickup (which is selected by the Multiplexer) are amplified by the Multiplexer to fit the effective range of ADC and stored in its memory. Each Multiplexer module has four inputs from electrodes with the same name of four different pickups, one output, and the calibration signal from the Synchronizer.

After storing the measured data required, the DSP (Digital Signal Processor) analyzes the measured data and transfers the results to the central computer. The processing module consists of four fast ADC, DSP, memory (RAM), and CAMAC interface. This process is synchronized by the signals of "start-stop" and "timing" from the synchronizer. These signals are triggered on the synchronization pulses from the Timer, which controls the gun modulator. The delay τ of the "timing" pulse in the interval of 90 ns (which is twice the interval of the synchronization pulses from the Timer) can be adjusted in the Synchronizer, with a discrete step of 1/256 (approximately 0.3 ns). The individual time delay (τ) for the channel and number of measurements (N) are setting in the Synchronizer and Timer modules before measurements. Synchronizer also provides the calibration pulses to the Multiplexers for gain calibration of the measurement channels.

3.7 Control system

3.7.1 Design of the control system

As shown in Figure 3.7.1, the control system can be divided into four main levels: display, control, access, and hardware. As like other experiments at KAERI, Lab Windows CVI will be used as a toolkit for developing control system user interface. In the control level, the central computer will retrieve database entries of monitored or

measured parameters, modify database entries of controlled parameters, and send new or modified parameters to the hardware devices. C or C++ will be used as a programming language in developing server and client software. In the control level, a widely used standard CAMAC crate will be used to control and monitor the hardware devices through multiple DAC and ADC, respectively.

The main idea in designing is dividing the control system into three groups: the injection, the acceleration, and the FEL control system. Each system will be controlled using three different computers. This scheme will prevent the computer from overloading, while allows the synchronization and interaction between different parts inside each system. Each system can be divided into several subsystems, such as, power supply, beam diagnostics, and so on.
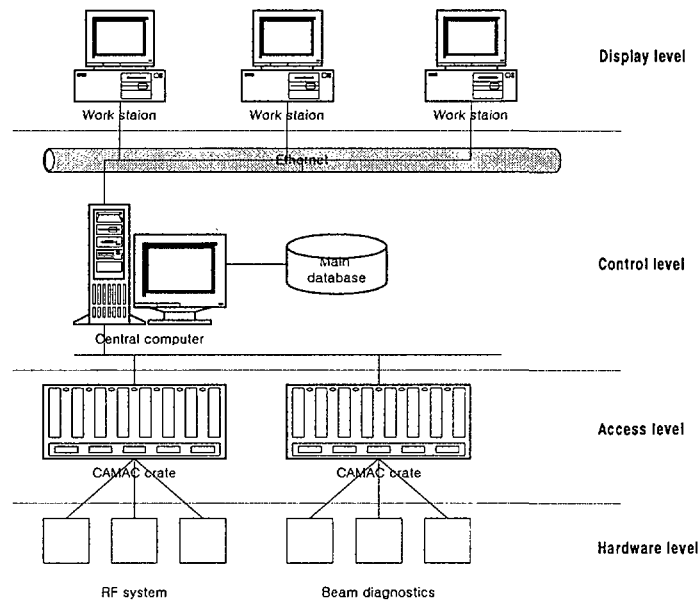
Figure 3.7.1 Schematic of the control system

3.7.2 Program structure

As we established in the injection control system, four types of the channels will be reserved in each central computer: a control, a monitoring, a back-coupling, and a threshold value control channel.

The control program consists of three main parts: server, client, and DDE-redirector. The server is responsible for executing all operational functions with

CAMAC modules, support of the channel databases, equipment tests, and so on. The client provides the mapping or displaying of all the information needed to user from the server and executes all the input data from the operator. The client and server are interacted each other through the DDE (Dynamic Data Exchange) mechanism. The DDE is the mechanism of data exchange between programs supported by MS window operating system. The DDE package includes the buffer for data and eight parameters including DDE link identificator. The redirector transfers this buffer and parameters, except for the identificator, from the client (or server) to the central computer redirector. The package with new identificator is transferred to the server (or client). This transfer is realized via TCP/IP at present. The use of Named Pipes is under consideration due to higher transfer rates.
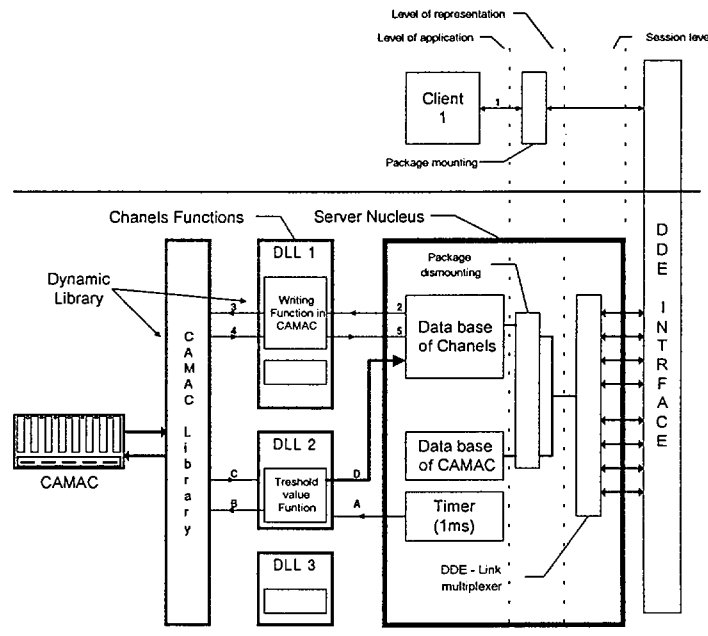
Figure 3.7.2. The structure of the client-server interaction

3.8 Safety aspects

The main constraint for accelerator installations is that the dose rate in an accessible area should be kept below 1 mrem/hr. Above this limit, access must be prohibited. For the safety, the interlock system combined with warning alarms should

be installed.

Table 3.8.1 Lists of the operating criteria and the shielding parameters.

Operating criteria	Electron energy	up to 100 MeV
	Electron energy in the dump (kinetic)	1.5 MeV
	Average current	up to 50 mA
	Total current losses	$< 5\ \mu A$
	Local losses at any point	$< 1.5\ \mu A$
Global shielding	1.5 m concrete wall	
	1 m concrete ceiling	
	15 mm lead door	
Local shielding	10 cm lead wall around the dump	

The building for the accelerators at KAERI is constructed with 1.5 m thick concrete walls and 1 m concrete ceiling, 19 cm brick in outside. The accelerators will be installed in the basement and the control room is located at the upstairs. Access to this building is regulated only to personnel who are working this area by personalized special card keys. The beam dump is locally shielded by 10 cm thick lead bricks and the interlock system stops the accelerators from operating whenever the access door is open and the level of current losses is above the threshold. The yellow Radiation warning signs are attached in all the radiation area. The initial data and general assumption is listed in Table 3.8.1. Each case the worst scenarios are evaluated

Dose rates due to bremsstrahlung and neutrons [3.8.1]

The dose rate at the maximum of the lost electron and from a high-Z target of optimal thickness can be estimated as following:

$$D_0 = 3\times10^4 \cdot E_0[\text{MeV}], \qquad [\text{rad} \cdot \text{m}^2/\text{hr/kW}]$$

$$= 3\times10^4 \cdot E_0^2[\text{MeV}] \cdot I[\text{mA}], \quad [\text{rad} \cdot \text{m}^2/\text{hr}], \qquad (3.8.1)$$

where E_0 is the energy of electrons in MeV and I is the current of the lost beam. The Dose rate from a low-Z target is less than that from a high-Z target. For a copper target it will be a factor of 0.7 and for an aluminum (metal) target, a factor of ~ 0.56. The dose rate due to the lost beam in aluminum vacuum chambers is estimated as 2.5×10^5 rad·m²/hr (using the data in Table 3.8.1).

The angular halfwidth of bremsstrahlung can be estimated as

$$\theta_{1/2} \cong 100/E_0 \cong 1° \cong 0.017.$$

The dose rate will be decreased as $\theta^{-3/2}$.

The bremsstrahlung from the dump is weakly directed. Its dose rate can be estimated as

$$D_0 = 2 \times 10^3 \cdot E_0^2/2 \cdot E_0 \cdot I \quad [\text{rad} \cdot \text{m}^2/\text{hr}], \tag{3.8.2}$$

where E_0 is in MeV and I is in mA. The denominator 2 is due to the dump made of the graphite. The dose rate at the dump is about 3.37×10^5 rad·m²/hr.

Neutrons production can be estimated as

$$\dot{N} = 0.5 \cdot 10^{12} \cdot E_0 I \cong 0.5 \cdot 10^{12} \cdot 100 \cdot 1.5 \cdot 10^{-3} \cong 7.5 \cdot 10^{10} \text{ s}^{-1}.$$

The conversion factor takes a value of

$$K_c \cong 10^8 \text{ m}^{-2} \cdot \text{s}^{-1} \cdot (\text{rem} \cdot \text{h}^{-1}).$$

Dose rates are ever estimated as

$$\dot{D}_\gamma = \dot{D}_0 \cdot \left(\frac{\vartheta_{1/2}}{\vartheta} \right)^{3/2} \cdot \frac{1}{r^2} \cdot k, \tag{3.8.3}$$

where θ is the minimum angle to the main maximum of the bremsstrahlung (this term is present if the observation point is out of the main maximum), r is the minimal distance from the point of loss to the point of observation, k is the total attenuation coefficient of the local and global shieldings (is taken from [3.8.1, p. 176]).

$$\dot{D}_n = \frac{\dot{N}}{4\pi r^2} \cdot \exp_{10}\left(-\sum_i \frac{h_i \cdot \rho_i}{\text{TVL}_i} \right) / K_c, \tag{3.8.4}$$

where h_i are the thickness' of shielding layers, ρ_i are their densities, TVL_i are their tenth value layers (are taken from [3.8.1, p. 195]).

The thickness of shielding for radiation is estimated by setting allowable dose rate as 10 mrem/week. r is assumed as 3 m (in worst case) and the local shielding at the dump is 10 cm lead. Then, the estimated thickness of the wall and the door needed is 92.8 cm of concrete and 10.4 cm of lead, respectively.

Ozone generation [3.8.2]

As the electron beam isn't extracted from the machine, only ozone production caused by bremsstrahlung is considered. As above, the bremsstrahlung from the dump and the high-energy current losses are discussed separately.

    a. Ozone from the dump.

As the dump is shielded locally, only the bremsstrahlung emitted through the holes in the shielding is sufficient for ozone production. The total visible solid angle of the holes is estimated as $\Omega \approx 0.01\pi$, the effective path length in air $L \approx 10$ m. Thus the

production of ozone is

$$p = 1.7 \cdot 10^{-4} \frac{\Omega}{4\pi} \cdot L \cdot W \approx 1.7 \cdot 10^{-4} \frac{0.01\pi}{4\pi} \cdot 10 \cdot 1.5 \cdot 5 \cong 3.2 \cdot 10^{-5} \, \text{l·min}^{-1}$$

$$\rightarrow 6.8 \cdot 10^{-5} \, \text{mg·min}^{-1}.$$

b. Ozone due to high-energy electron losses.

In this case the main maximum of the bremsstrahlung is shielded by magnetic circuits of the bending magnets, so the production of ozone is

$$p = 1.7 \cdot 10^{-4} \cdot L \cdot W \cdot k \approx 1.7 \cdot 10^{-4} \cdot 10 \cdot 100 \cdot 5 \cdot 10^{-3} \cdot 1.5 \cdot 10^{-2} \cong 1.3 \cdot 10^{-5} \, \text{l·min}^{-1}$$

$$\rightarrow 2.7 \cdot 10^{-5} \, \text{mg·min}^{-1}.$$

Totally

$$p_\Sigma \approx 9.5 \cdot 10^{-5} \, \text{mg·min}^{-1}.$$

Assuming the decomposition time $T = 50$ min, the volume of the accelerator room $V = 30.5 \cdot 12.5 \cdot 3.8$ m^3, and the threshold limit value TLV $= 0.1$ mg·m^{-3}, one obtains the saturation concentration

$$p = \frac{p_\Sigma \cdot T}{V} \approx \frac{9.5 \cdot 10^{-5} \cdot 50}{30.5 \cdot 12.5 \cdot 3.8} \cong 3.3 \cdot 10^{-6} \, \text{mg·m}^{-3} \rightarrow 3.3 \cdot 10^{-5} \, \text{TLV}$$

even without ventilation.

Air activation

For air activation only ^{13}N and ^{15}O isotopes are significant as the activity production rates for other isotopes are much less. As the threshold energies of the isotope generation are 10.55 and 15.67 MeV respectively [3.8.1], only the high-energy electrons losses can produce these isotopes. According to [3.8.1] one can find the saturation activities as

^{13}N: $A_i = \kappa \cdot L \cdot W \cdot k \cong 1.4 \cdot 10^4 \cdot 10 \cdot 100 \cdot 5 \cdot 10^{-3} \cdot 1.5 \cdot 10^{-2} \cong 10^3 \, \mu\text{Ci}$,

^{15}O: $A_i \cong 1.500 \cdot 10 \cdot 100 \cdot 5 \cdot 10^{-3} \cdot 1.5 \cdot 10^{-2} \cong 110 \, \mu\text{Ci}$.

Even without ventilation the saturation concentrations are less than the maximum permissible concentrations (MPC) $2 \cdot 10^{-6}$ Ci·m^{-3}

^{13}N: $A_i / V \cong 7 \cdot 10^{-7}$ Ci·m^{-3},

^{15}O: $A_i / V \cong 7.6 \cdot 10^{-8}$ Ci·m^{-3}.

Activation of components

Parts of the accelerator system are activated by a bremsstrahlung and neutrons from the lost high energy electrons. As the exact evaluation of the induced activity is too complicated and not reliable, let's estimate the activity analogous to the estimations in the reference [3.8.3]. The maximum saturation dose rate at the distance of 0.5 m from

the machine in that case is $D_0 = 0.5$ μrem·s^{-1} if the operating mode is: $E_0 = 200$ MeV, lost electrons rate $\Phi_0 = 3 \cdot 10^{10}$ s^{-1}. In our case the maximum energy is twice less and the $\Phi = 5 \cdot 10^{-6} / 1.6 \cdot 10^{-19} \cong 3.1 \cdot 10^{13}$. So the expected dose rate is

$$D \cong D_0 \cdot \frac{E}{E_0} \cdot \frac{\Phi}{\Phi_0} \cong 0.5 \cdot \frac{100}{200} \cdot \frac{3.1 \cdot 10^{13}}{3 \cdot 10^{10}} \cong 260 \ \mu\text{rem·s}^{-1} \rightarrow 0.93 \ \text{rem·h}^{-1},$$

if all the electrons lost at one point (in worst senarios). Suggesting the losses are uniform over the 100 MeV track (a more realistic assumption) of length $\cong 25$ m, one obtains

$$D \cong 0.93 \cdot \frac{0.5}{25} \cong 0.019 \ \text{rem·h}^{-1}.$$

It's clear that 24 hours after switching off the machine the dose rate is ten times less. So to estimate the real dose rate one has to take the average lost electrons rate over sufficient period (say, 24 hours). For example, if the accelerator system operates one hour per day, the estimated dose rates are 0.039 and $7.8 \cdot 10^{-4}$ rem·h^{-1} respectively. It can be serious if the machine has been operating continuously long time before the damage.

All these problems can be solved if the current losses at high energy are decreased sufficiently.

References.

[3.3.1] Enrico Chiaveri, 5th European Particle Accelerator Conference - EPAC '96 Sitges, Barcelona, Spain, 200 (1996)

[3.4.1] Thomson tubes electroniques, "Preliminary Information for a 200 kW CW RF power source", private communication with Thomson tube company.

[3.4.2] S. Simrock, CEBAF PR-89 (1989)

[3.6.1] Particles and Fields series 46, Accelerator Instruments (1991)

[3.8.1] W.P.Swanson. Radiological safety aspects of the operation of electron linear accelerators. IAEA, Vienna, 1979.

[3.8.2] W.P.Swanson. Toxic gas production at electron linear accelerators. Stanford, California, 1980.

[3.8.3] Explanation document to displacement and shielding of the VEPP-3 collider. BINP, Novosibirsk, Russia, 1969.

4. Advanced Quantum Beam Sources

4.1 Free Electron Laser

4.1.1 System configurations

For a design of a free-electron laser (FEL) the parameters of the electron beam should be defined. However, for the preliminary design of the FEL the electron beam parameters of the injector are used, since the conceptual design of the accelerator is not completed.

The schematics of FEL systems are shown in Figure 3.1.2. The FEL-I for mid infrared to far infrared is located in the first recirculation track with the bypass magnets. This system uses the electron energy of 20 – 35 MeV. During the bypass to the FEL, the phase of the electron beam should be delayed by half wavelength of the RF for the deceleration mode. It will be the first step for high power FEL demonstration with the energy recovery. The IR FEL system is located in the 3rd track of the recirculation beam line. The followings are summarized parameters of the electron beam for the FEL design.

1. FEL-I (MIR/FIR FEL)
   - Electron beam energy   :   20 – 35 MeV
   - Electron current
     - Peak current   :   20 A for 30 ps pulsewidth
     - Average current   :   10 mA, max.
   - Energy spread of the beam: 0.5%
   - Repetition rate   :   22 MHz, max.
   - Normalized emittance   :   150 π mm mrad

2. FEL-II (IR FEL)
   - Electron beam energy   :   60 – 100 MeV
   - Electron current
     - Peak current   :   20 A for 30 ps pulsewidth
     - Average current   :   10 mA, max.
   - Energy spread of the beam: 0.2%
   - Repetition rate   :   22 MHz, max.
   - Normalized emittance   :   150 π mm mrad

The energy range of the accelerator system is not specified now. However, we will try to get the wide range energy tunability during designing the system.

The main parameters of the FEL-I and FEL-II can be determined from the needs of applications. When we consider the recirculation of the electron beam for energy recovery, the extraction ratio of the optical light from the electron beam should not exceed 1% due to low energy of the injection. We want to extract the optical power of 0.1 – 1% from the electron beam. In this case the optical power would be 1 – 10 kW in average mode.

The main parameters of the FEL-I and FEL-II are as follows.

1. FEL-I (MIR/FIR FEL)
   - Wavelength   :   5 - 16 μm
   - Laser power
        Peak power   :   1 MW for 30 ps pulsewidth
        Average power   :   1 kW, max.
   - Spectral width, $\Delta\lambda/\lambda$:   < 0.05%

2. FEL-II (IR FEL)
   - Wavelength   :   1 – 5 μm
   - Laser power
        Peak power   :   5 MW for 30 ps pulsewidth
        Average power   :   5 kW, max.
   - Spectral width, $\Delta\lambda/\lambda$:   0.01%

4.1.2 Undulators

Combined with desirable parameters of the FEL systems, undulators for the FEL-I and FEL-II have been designed conceptually. The main parameters of the undulator are period, magnetic strength, total length, and gap distance. We have used electromagnetic schemes for the undulators to get high quality distribution of the field and tune magnetic strength in wide range.

The followings are main parameters of the planar undulators.

1. Undulator-I (MIR/FIR FEL)
   - Period   : 35 mm
   - Peak strength : 1.5 – 3.0 kG

- Number of periods : 60
- Gap distance : 20 mm
- Type : Permanent magnet assisted electromagnetic undulator

2. Undulator-II (IR FEL)
   - Period : 72 mm
   - Peak strength : 0 – 2.0 kG
   - Number of periods : 40
   - Gap distance : 30 mm
   - Type : Pure electromagnetic undulator

There are several important requirements in the design of the undulators. The electron beam in undulator should meet the following coherence requirements on the deviation and angle of the electron trajectories from center axis.

$$\sigma_e < \sqrt{\frac{L\lambda}{4\pi}} = 0.9 \text{ mm} \quad \text{(for Undulator-I)}$$
$$= 0.5 \text{ mm} \quad \text{(for Undulator-II)}$$

$$\sigma_e' < \sqrt{\frac{\lambda}{L}} = 1.5 \text{ mrad} \quad \text{(for Undulator-I)}$$
$$= 0.6 \text{ mrad} \quad \text{(for Undulator-II)}$$

L is total length of the undulator and λ is wavelength of the radiation. The condition should be satisfied with limited values of the first and second integrals of the undulator field. The requirements on the integrals can be expressed as follows.

$$\delta\left(\int B_y dz\right) < \frac{m_e \gamma \beta c}{e} \sqrt{\frac{\lambda}{L}} = 30 \ G \cdot cm \quad \text{(for Undulator-I)}$$
$$= 15 \ G \cdot cm \quad \text{(for Undulator-II)},$$

and

$$\delta\left(\iint B_y dz^2\right) < \frac{m_e \gamma \beta c}{2\pi e} \sqrt{\lambda L} = 1400 \ G \cdot cm^2 \quad \text{(for Undulator-I)}$$
$$= 800 \ G \cdot cm^2 \quad \text{(forUndulator-II)},$$

where B_y is the magnetic field component in vertical direction when poles are placed

with the same direction and m_e is the rest mass of an electron.

The longitudinal structure of the iron pole is designed to have minimum harmonic amplitudes of the undulator field at the center axis. To meet the requirement the pole thickness should be 1/3 of the undulator period. In the case of the Undulator-I, we can not satisfy the condition because wide tuning range of the field strength needs much thicker pole. However, we modify the edge shape of the pole and the 3rd harmonics of the field is calculated to be less than 0.1% of the fundamental amplitude.
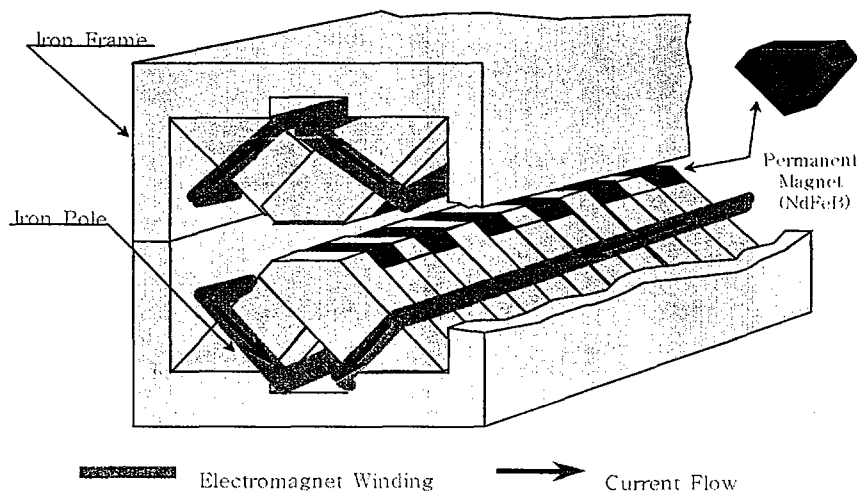
Figure 4.1.1 Schematic diagram of the Undulator-I for the MIR/FIR FEL.

Figure 4.1.1 shows the schematic diagram of the Undulator-I. To increase the field strength in the gap space, the magnetic induction in the iron poles should be less than saturation value. To solve that problem the material of the iron poles should have enough value of permeability for strong magnetic induction. The other way is to compensate the magnetic induction in the poles with the field of opposite direction. We have used permanent magnets for the compensation. It was tested that the field strength of the undulator can be stronger than that of hybrid configuration. The longitudinal structure of the undulator is shown in Figure 4.1.2 with the magnetic field distribution. Figure 4.1.3 shows calculated magnetic field strength of the Undulator-I as a function of the applied current. The cross-sectional view of the designed undulator is shown in Figure 4.1.4. With the same configuration we have developed a high accuracy undulator having field error of 0.01%.
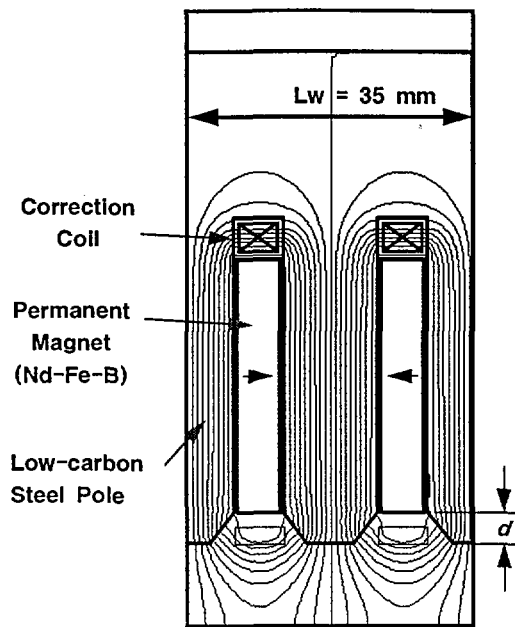
Figure 4.1.2 Longitudinal structure of the Undulator-I with the magnetic field distribution.
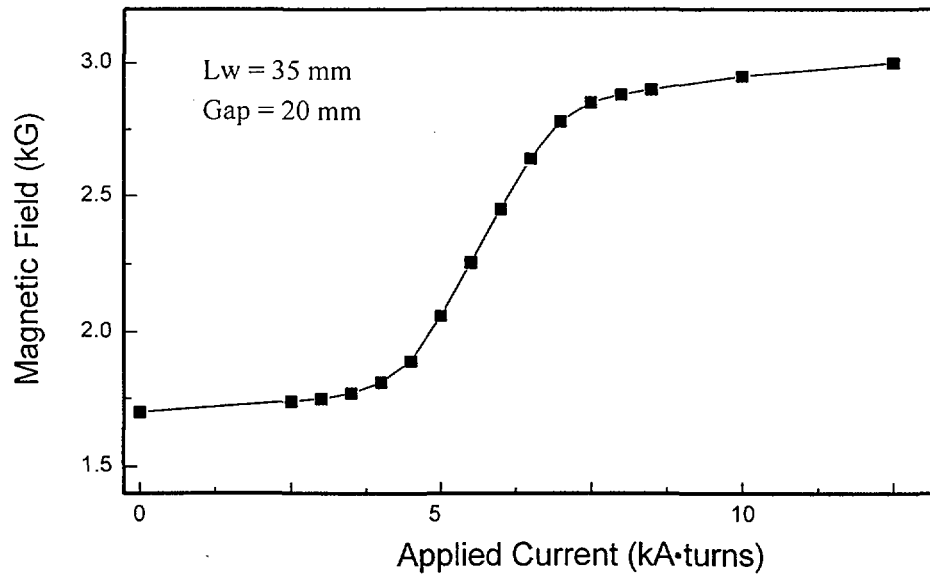
Figure 4.1.3 Calculated magnetic field strength of the Undulator-I as a function of the applied current
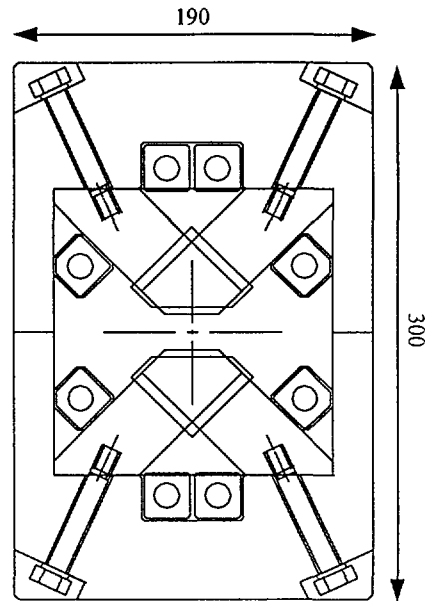
Figure 4.1.4 Cross-sectional view of the Undulator-I.
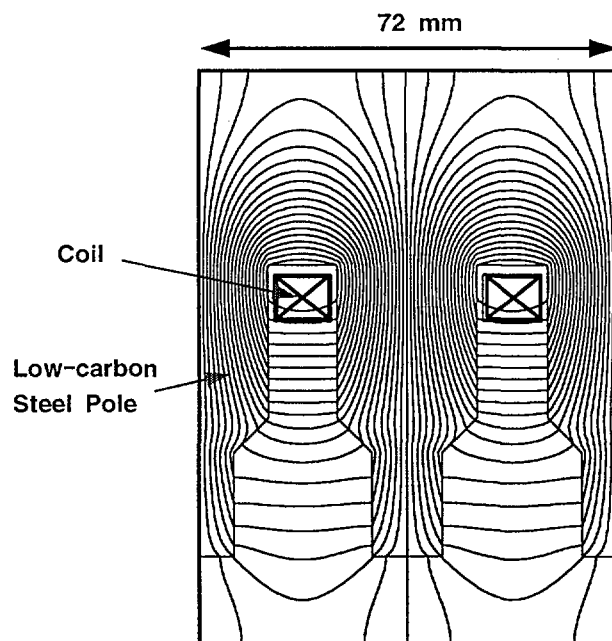
Figure 4.1.5 Longitudinal structure of the Undulator-II
with the magnetic field distribution.

Figure 4.1.5 shows the longitudinal structure of the Undulator-II with the equipotential field lines. It is a pure electromagnetic undulator. The thickness of the pole is 12 mm to reduce third harmonics of the magnetic field at center axis of the undulator. The maximum field strength is 2 kG with the current of 1 kA in 8 turn coil. To satisfy the required condition for the field distribution, correction coils are used in every pole.

4.1.3 Optical resonators

To provide the synchronism condition it is necessary that the length of the resonator should be the half integer of the distance between electron bunches. The cavity length of 27.25 m is the best choice since it satisfies the minimum repetition rate of 5.5 MHz. We considered several points for the design of the resonators.

- The spot size of the light on the mirrors should be larger than 4 cm in diameter.
- The loss of the fundamental mode at the ends of undulator should be less than 10^{-4}.
- The possibility of Compton back scattering between FEL beam and electron bunches should be taken into account.

The possibility of the Compton back scattering in the resonator needs a resonator length more than 2 times of the minimum value by the bunch repetition rate. 27.25 m long optical resonator is good enough to operate the Compton backscattering scheme, except for the operation with the repetition rate of 5.5 MHz. The condition of the larger light diameter on the mirror also needs an enough length of the resonator. The followings are the main parameters of the resonators for FEL-I and FEL-II.

1. Resonator-I (MIR/FIR FEL)
    - Length : 27250 mm
    - Resonator type : Near concentric
    - Curvature of the mirrors : 13630 mm
    - Mirror diameter : 300 mm
    - Mode radius (e^{-1} point of maximum)
        - Waist : 0.6 – 1.2 mm
        - Ends of undulator : 2.4 – 4.8 mm
        - Mirrors : 30 – 60 mm

- Diffraction loss	:	$< 10^{-4}$
- Out coupling ratio	:	10%
- Mirror material	:	Water cooled copper

2. Resonator-II (IR FEL)

- Length	:	27250 mm
- Resonator type	:	Near concentric
- Curvature of the mirrors	:	13625 mm
- Mirror diameter	:	200 mm
- Mode radius (e^{-1} point of maximum)		
Waist	:	0.25 – 0.5 mm
Ends of undulator	:	2.1 – 4.4 mm
Mirrors	:	20 - 40 mm
- Diffraction loss	:	$< 10^{-5}$
- Reflectance of the mirrors		
Full mirror	:	>99.5%
Out coupling mirror	:	90 - 98%
- Mirror material	:	Dielectric coated CaF_2

Thermal distortion of the mirrors should be studied. Out coupling method of the Resonator-I is not determined yet. We are considering several ways and spatial distribution of the out coupled light would be important for the consideration.

4.1.4 Applications

The FEL system is dedicated to the applications of photochemical research for isotope separation, spectroscopic study on solid-state materials, biological and medical researches, and material processing.

Tunable high power laser in IR region is very useful for the study on multi-photon dissociation (MPD) of various kinds of molecular. One of the attractive field among them is the isotope separation of valuable elements using selective dissociation with the tunable laser. The study and trials of the isotope separation has been attempted mainly by using CO_2 and CO lasers. Recently, FEL is considered as an ideal source for the work with its continuous tunability and high power capability.

The followings are summarized contents of the application. Here, the photochemical process and wavelength for the process are only example on the basis of the previous studies. We expect that more efficient processes can be developed by further study with the FEL.

1. ^{10}B

 - Natural abundance : 19.9%

 - Photochemical process : $^{10}BCl_3 + nh\nu \rightarrow {}^{10}BCl_2 + Cl$

 - Wavelength : 8 – 11 μm
 - Use : Neutron absorption material in reactor

2. ^{28}Si

 - Natural abundance : 92.2%

 - Photochemical process : $^{28}Si_2F_6 + nh\nu \rightarrow {}^{28}SiF_4 + {}^{28}SiF_2$

 - Wavelength : 10 – 13 μm
 - Use : High-density semiconductor material

3. ^{30}Si

 - Natural abundance : 3.1%

 - Photochemical process : $^{30}Si_2F_6 + nh\nu \rightarrow {}^{30}SiF_4 + {}^{30}SiF_2$

 - Wavelength : 10 – 13 μm
 - Use : Material for fusion reactor

4. ^{235}U

 - Natural abundance : 0.72%

 - Photochemical process : $^{235}UF_6 + nh\nu \rightarrow {}^{235}UF_5 + F$

 - Wavelength : 7 – 16 μm
 - Use : Fuel for nuclear reactor

5. ^{13}C

 - Natural abundance : 1.1%

 - Photochemical process : $^{13}CHBrF_2 + nh\nu \rightarrow {}^{10}CF_2 + HBr$

 - Wavelength : 3 – 11 μm
 - Use : Tracer

6. ^{18}O

 - Natural abundance : 0.2%

 - Photochemical process : $HC^{18}OOH + nh\nu \rightarrow C^{18}O + H_2O$

  - Wavelength   : 3 – 6 μm
  - Use   : Tracer

7. ^{15}N

  - Natural abundance : 0.4%
  - Photochemical process : $CH_3{}^{15}NO + nh\nu \rightarrow {}^{10}NO + CH_3$
  - Wavelength   : 3 – 6 μm
  - Use   : Tracer

Spectroscopic study with tunable source of IR/MIR range can be used for determining the behavior and performances of an entire class of semiconductor devices. And the FEL has great potential for researchers who are focusing on the field of bio-molecular operation including photo-chemical processes. The followings are main contents of the FEL applications for semiconductor, biomedical work, and next generation technology of material processing.

1. Semiconductor and solid-state physics
   - Measurement of band structures of semiconductor heterojunctions
   - Development of terahertz devices
     - Optically detected terahertz resonance
     - Terahertz side band generation
   - Studies on quantum-well devices
     - Intersubband studies on AlGaAs/GaAs quantum well
     - Resonant tunneling through semi-metal quantum wells
     - Nonlinear quantum dynamics in quantum wells
     - Photocurrent dynamics in quantum well photodetectors
   - Studies on high T_c superconducting materials
   - Luminescent spectroscopy on solid samples
   - Studies on surface electromagnetic wave

2. Biomedical technology
   - Selective ablation of targeted material in human body
     - Removal of cholesterol esters from an arteriosclerotic region
     - Tissue removal : Laser mess
     - Ablation of corneal stroma
     - Ablation of neural tissue
   - Surface modification of tooth dentine

- Light-activated chemo-therapy for cancer
- Imaging of living cells with scanning near-field IR microscopy
- Vibrational echo study of myoglobin

3. Material processing
   - Annealing of diamond
   - Crystallization of amorphous SiC
   - Silicon nanostructure fabrication
   - Deposition of carbon thin film
   - Large area thermal processing
     - Polymer surface processing
     - Metal surface processing
   - Precision materials removal

4. Others
   - Monitoring of air pollutants
   - Spectroscopy on gas-phase molecules
   - IR/FIR tomography
   - Damage effect on electro-optic devices

4.2 Compton X-ray and γ-ray Source

4.2.1 Compton backscattering

Compton backscattering of laser light from a relativistic electron beam was proposed as a method of generating quasi-monochromatic, polarized photons in 1963 [4.3.1, 4.3.2]. From the four-momentum conservation law, the energy of the scattered photon is derived as [4.3.3]:

$$\hbar\omega' = \hbar\omega \frac{1 - \beta\cos\theta_i}{1 - \beta\cos\theta_f + \frac{\hbar\omega}{E_e}(1 - \cos\theta_{ph})} \tag{4.3.1}$$

where ω and ω' are the frequencies of incoming photon and outgoing (scattered) photon respectively and E_e is the energy of incoming electron. θ_i (or θ_f) the angle between incoming electron and incoming (or outgoing) photon and θ_{ph} is between incoming and outgoing photons. The peak energy of scattered photons reaches its maximum in

forward direction and in head-on collision. The differential cross section for unpolarized electrons and photons is giving by

$$d\overline{\sigma} = 8\pi r_e^2 \frac{dy}{x^2} \left\{ \left(\frac{1}{x} - \frac{1}{y} \right)^2 + \left(\frac{1}{x} - \frac{1}{y} \right) + \frac{1}{4} \left(\frac{x}{y} + \frac{y}{x} \right) \right\},$$ (4.3.2)

where

$$x = \frac{2\gamma\hbar\omega(1 - \beta\cos\theta_i)}{mc^2} \quad \text{and} \quad y = \frac{2\gamma\hbar\omega'(1 - \beta\cos\theta_f)}{mc^2}.$$

Thus, the total cross section becomes

$$\sigma_{tot} = \frac{2\pi r_e^2}{x} \left\{ \left(1 - \frac{4}{x} - \frac{8}{x^2} \right) \ln(1 + x) + \frac{1}{2} + \frac{8}{x} - \frac{1}{2(1 + x)^2} \right\}.$$ (4.3.3)

For the scattering of polarized photons by unpolarized electrons, the scattering cross section summed over all polarizations of the outgoing photons is [Landau 1982]

$$d\sigma = d\overline{\sigma} - \frac{4r_e^2 dy d\varphi}{x^2} \xi_3 \left[\left(\frac{1}{x} - \frac{1}{y} \right)^2 + \left(\frac{1}{x} - \frac{1}{y} \right) \right],$$ (4.3.4)

where ξ_3 is one of components of the Stokes parameters of the incoming photons, $\xi = (\xi_1, \xi_2, \xi_3)$. There is only one linear polarization parameter ξ_3 for the incoming photon. $\xi_3 = 0$ describes the circular polarization case, which corresponds to the scattering cross section of unpolarized electrons and photons.

The total number of scattered photons per collision between the electron and photon bunch is governed by [4.3.4, 4.3.5]

$$v_b = N_e N_{ph} c \iiint \int dp^3 dk^3 dV dt \, \sigma(\vec{p}, \vec{k}) |1 - \beta\cos\theta_i| f_e(\vec{r}, \vec{p}, t) f_{ph}(\vec{r}, \vec{k}, t).$$ (4.3.5)

where $f_e(\vec{r}, \vec{p}, t)$ and $f_{ph}(\vec{r}, \vec{k}, t)$ are the normalized distribution functions of electrons and photons in the phase space respectively. If the collisions occur periodically with frequency f_c, the total flux of scattered photons becomes

$$\dot{N} = f_c v_b.$$ (4.3.6)

Assume that the electron beam has a paraxial Gaussian distribution in the collision region and the rate of the collision is equal to the repetition rate of electron bunches. In a head-on collision, the total flux can be reduced to a simple form:

$$\dot{N}_{scatt} = f_c \frac{\sigma_{tot}}{A} N_e N_{ph},$$ (4.3.7)

where A is the effective overlap area and N_e (or N_{ph}) is the number of electrons (or photons) per pulse. When the collision occurs at the waist of both beams, the effective overlap is

$$A \cong \frac{\lambda\beta_0}{2} \sqrt{1 + \frac{4\pi\varepsilon_x\beta_x}{\lambda\beta_0}} \sqrt{1 + \frac{4\pi\varepsilon_y\beta_y}{\lambda\beta_0}}$$ (4.3.8)

where $\varepsilon_{x,y}$ are the transverse emittances of the electron beam, $\beta_{x,y}$ are the transverse beta functions at $z = 0$ (collision point), and β_0 is the Rayleigh range of the photon beam. The electron beam current and the laser power are main factors for high flux of the scattered photons.

The quality of the scattered photons is determined dominantly by the quality of the electron beam when the recoil parameter is small. In an ideal case (no energy spread and no angular spread), the scattered beam energy is determined by the observation angle. In reality, the energy resolution and energy distributions of scattered photons are mostly affected by the electron beam quality, in particular, the energy spread and angular spread of the electron beam. The initial collision angle θ_i influences mainly to the peak energy of the scattered photons and the contribution to the energy resolution of θ_i is negligible for well-collimated Gaussian beams. Assuming the size and position of the collimator in front of a detector is optimized, the energy resolution of scattered beams can be approximately obtained as like:

$$\frac{\sigma_{E_{scatt}}}{E_{scatt}} \cong \sqrt{\left(\gamma^2\theta_j^2\right)^2 + \left(2\frac{\sigma_E}{E}\right)^2} \cong \sqrt{\left(\frac{\gamma^2\varepsilon_x}{\beta_x}\right)^2 + \left(\frac{\gamma^2\varepsilon_y}{\beta_y}\right)^2 + \left(2\frac{\sigma_E}{E}\right)^2}.$$ (4.3.9)

Since the energy spread and the normalized emittance of the electron beam is 0.2 % and 150π mm·mrad, respectively, the energy resolution of the scattered photons is mostly determined by the angular spread of the electron beam. However, when the design value of 40π mm·mrad is achieved after completing the acceleration system, the energy spread can be reduced by a factor of 4. In order to increase the energy resolution, the beta function at the collision point should be increased. In case of Compton scattering with the external laser, it is easy to change the Rayleigh range of laser and the beta function of the electron beam, but, with the FEL, it is not easy. However, the FEL mode can generate more flux than the external laser mode due to high intracavity power of the FEL mode. Therefore, we can select the external laser mode or the FEL mode depending on the applications

4.2.2 Compton scattering with the external laser

As mentioned in Section 4.1.3, the cavity length is 27.25 m. The external laser light will enter through the periscope located in the downstream and the Rayleigh range and the beam waist will be adjusted using the beam expander placed in between the periscope and the external laser. Table 4.2.1 shows the tunable range of scattered photons and Table 4.2.2 illustrates the expected values of the total flux and energy resolution, as an example. The CW mode-locked Nd:YLF laser will be used as a first light source to generate X-rays up to 180 keV. For γ-ray generation, the electron beam will be accelerated up to 200 MeV and UV N_2 laser will be used for the collision.

Table 4.2.1 The possible energy of scattered photons in the external laser mode

e-beam energy lasers	35 MeV	100 MeV	200 MeV
Nd:YLF laser (1.053 μm)	22.1 keV	180 keV	0.72 MeV
UV N_2 laser (337 nm)	68.9 keV	0.56 MeV	2.23 MeV

Table 4.2.2 The expected flux and energy resolution of x-rays
in the external laser mode

Laser	wavelength [μm]	1.053
	average power [watt]	20 @ 100 MHz rep.rate
	repetition rate [MHz]	88
Electron beam	energy [MeV]	100
	current [mA]	10
	energy spread [%]	0.2
	normalized emittance [mm·mrad]	150π
X-rays	energy [keV]	180
	total flux [/sec]	~ 10^6
	energy resolution, FWHM, [%]	~ 2 − 4*

* : The energy resolution can be changed depending on the Rayleigh range of laser and the beta function of electron beam.

In the external laser mode, the collision point can be increased at least up to 8 points, by changing the Rayleigh range of laser and the beta function of electron beams and the repetition rate of both beams. The energy resolution mainly determined by the beta function of electron beams at the collision point rather than the energy spread in our machine. Since it is quite easy to change the Rayleigh range of laser and the beta function of electron beam in the external mode, the external mode will generate X-rays or γ-rays with better resolution at the expense of low flux, compared to the FEL mode. But the tunable range is much narrower than that in the FEL mode.

4.2.3 Compton scattering with the FEL

Compared to the external mode, the FEL mode has two main advantages: the usage of high intracavity power and the tunability. As shown in Table 4.2.3 and 4.2.4, the

Table 4.2.3 The tunable range of scattered photons in the FEL mode

Electron beam energy	~ 35 MeV	~ 100 MeV	~ 200 MeV
FEL	5 ~ 16 μm	1 ~ 5 μm	0.25 ~ 1.2 μm
X-rays or γ- rays	1.5 ~ 4.7 keV	38 ~ 190 keV	0.6 ~ 3 MeV

Table 4.2.4. The expected flux and energy resolution of X-rays in the FEL mode

FEL	wavelength [μm]	2
	average power [kilowatt]	2
	repetition rate [MHz]	5.5 ~ 22
Electron beam	energy [MeV]	100
	current [mA]	10
	energy spread [%]	0.2
	normalized emittance [mm·mrad]	150π
X-rays	energy [keV]	180
	total flux [/sec]	$10^7 \sim 10^9$
	energy resolution, FWHM, [%]	$\sim 1 - 4^*$

* : The energy resolution can be changed depending on the Rayleigh range of laser and the beta function of electron beam.

tunable range is wider and the total flux is two or three order higher than that in the external mode. But, the disadvantage is large energy spread of the scattered photon beams. In Compton scattering experiments, we need to adjust the beta function of electron beam to optimize the energy resolution and the total flux of scattered photon beams as well as the FEL gain. (since the Rayleigh range can not be changed once the cavity mirrors are installed.) As like the external laser mode, the energy of electron beam will be increased up to 200 MeV for low energy γ-ray generation for the nuclear physics (for example, nuclear resonance fluorescence). The conceptual design for optimizations including the possible or optimal collision points is underway.

4.2.4 Applications

The Compton scattering scheme at AQBS can provide photons ranging from soft x-rays to low energy γ-rays. Since the brightness of x-ray and γ-ray sources generated via Compton backscattering scheme is high, we can use variety of applications, such as, holography or tomography of biological tissue, lithography, spectroscopy, nuclear resonance fluorescence, and so on. By increasing the electron beam current up to order of hundreds of mA, these sources can be used for the cancer therapy which is needed at least total flux of ~ 10^{11} /sec.

4.3 High-Current Electron Beam Source

4.3.1 E-beam irradiation port

Design of electron beam irradiation port depends on specific applications, the beam port, however, must meet basic requirements such as low loss of electron beam current, high radiation and heat resistivity as well as suitable mechanical strength under heavy-duty operations. Besides projectile electron itself, the bremsstrahlung photons can yield secondary radiation sources such as neutrons, positrons, secondary electrons, and high-energy photons. The choice of a beam window material and the window design should be determined by the thermomechanical properties of the window material, since the beam power dissipation at the window leads to high power density on the small spot of the window. Power density on the spot can be reduced by expanding the beam size, since it is inversely proportional to the square of beam radius. The most common window materials are composed of *Ti* and *Al* for electron beams.

4.3.2 Applications of electron beam

Utilizing the energy of the electron beam, we can modify the target material by heating or by altering chemical bonds. In most cases a focused beam is used. Depending on the application, the beam parameters, such as, power density, total beam power, acceleration voltage (which determines the penetration depth), and beam diameter, are easily adjustable. Since the electron beam is capable of delivering its power directly to the material or target zone, utilities of electron beam can be found in processing high melting point and reactive materials, including alloys and compounds. Electron beam melting can be used for refining refractory metals and reactive metals by keeping them in molten state in vacuum while impurities evaporate. In semiconductor industry, electron beam evaporation technique is used to produce metal and dielectric coatings, such as, antireflection coating on optical lenses or mirrors. High-density electron beam can be used in welding process requiring both high depth-to-width ratio of the welding seams and low thermal distortions around the seam. High power pulsed electron beam can also drill the material by making holes and cavities of controlled depth.

In the semiconductor industry, micro fabrication of semiconductor can be performed by electron beam lithography with the high degree of flexibility, accuracy, and speed. This method will inscribe the original patterns directly on substrate. For the electron beam lithography, the substrate must be coated with a thin film of radiation sensitive material called a resist. The electron beam irradiation changes the chemical solubility of the resist in the exposed area. Subsequently, in a developed step, the more soluble part of the resist gets removed and a pattern stays behind. This residual resist plays a role of a mask in transferring the pattern to the substrate, either by etching, deposition, or ion implantation.

Industrial applications of accelerators can be found in variety fields of radiation processing. Radiation sterilization is basically a cold method that is attractive in processing sealed medical supplies and packaged food products because of good penetrating power of high energy electron beams. Application of ionizing radiation technique to polymers makes it possible to form additional bonds between long chains in polymer, as a result of the cross-linked structure, the polymers can have higher resistance to temperature and solvents. The ionizing radiation method can also be used to degrade the polymers, instead, for giving special properties to the material. Other radiation-induced polymerizations can be found in curing of coatings and treating textile fibers.

Table 4.3.1 Electron beam energy requirements for various industrial applications.

Application Field	Examples of Applications	Beam Energy
Sterilization	Medical supplies Pharmaceutical Products Food Preservation Quarantine of imported agricultural product	1~10 MeV
Material Processing	Melting Refining Enhancement of corrosion/erosion resistance	1~10 MeV
Environmental Protection	Removal of NO_x, SO_x from combustion gas Decontaminate pesticide/toxic material in soil Removal of heavy metal pollutants in waste water	1~5 MeV
Semiconductor	Micro fabrication Lithography Controlling switching time of thyristor Amorphization of silicone	1.5~3 MeV
Welding	Metal Alloys Plastics	0.5~ 3 MeV
Polymerization	Enhancement of durability of rubber product Teflon degradation Surface treatment of fabrics	< 1 MeV

4.4 Neutron Beam Source

4.4.1 Neutron production based on electron accelerator

An accelerator can provide the most efficient neutron sources with high energy-resolution covering a wide range of the neutron energy. Time of flight method requires the electron beam pulses of microsecond and nanosecond for resolving neutron energies in eV and MeV regions, respectively. Since the narrower pulses may yield low neutron intensities, in the high-energy region, it is desirable to increase the electron beam intensity to improve the neutron energy resolution. Thus a linear type of accelerators has advantages over circular types in producing higher peak currents and flexibility in tuning pulse duration and repetition rate. Typical projectiles for an accelerator are electrons, protons, and deuterons. Neutron production process of the electron beam in thick heavy target material is based on following steps; electron-

photon cascades, photonuclear reactions initiated by γ-rays due to bremsstrahlung, and emission of nucleons from evaporated nuclei. Since the bremsstrahlung yield is proportional to Z^2, the target material needs to be composed of elements having high atomic number. Photonuclear reactions are always endothermal and the spectrum of the nucleons produced is continuous. The charge neutrality enables neutrons to escape more likely than protons from nucleus.

To get neutrons form evaporation process, a range of the required electron beam energy is 20 MeV~100 MeV. The optimal energy range of the electron beam is 30~40 MeV, since the neutron yield is getting to saturate and the majority of electron beam energy converts into heat deposited in the target above this energy range. Thus, above 100 MeV, it is better to exploit spallation reaction, not applicable with electron beam, but with proton or deuteron beam. Neutron yield depends on the type of target material as well as the beam energy and current. Typical neutron yield is about 7.56×10^{-3} n/s with a single 35 MeV electron impinging on Pb target. Thus we plan to produce 1.41×10^{14} n/s from the Pb target by operating the linac with average beam current of 3 mA at 35 MeV. The range of neutron spectra from the evaporation process is 50 KeV~2 MeV. To get thermal spectrum, an assembly of moderator needs to be placed around the target.

Table 4.4.1 Neutron yields by single electron impinging on various targets.

Beam Energy	Lead (Pb)	Tantalum (Ta)	Uranium (^{238}U)	Uranium (^{235}U)
20 MeV	2.30×10^{-3} n/s	2.50×10^{-3} n/s	5.18×10^{-3} n/s	6.05×10^{-3} n/s
30 MeV	6.48×10^{-3} n/s	7.38×10^{-3} n/s	1.31×10^{-2} n/s	1.46×10^{-2} n/s
35 MeV	7.56×10^{-3} n/s	7.73×10^{-3} n/s	1.73×10^{-2} n/s	2.07×10^{-2} n/s
40 MeV	8.67×10^{-3} n/s	1.07×10^{-2} n/s	1.98×10^{-2} n/s	2.37×10^{-2} n/s
50 MeV	1.12×10^{-2} n/s	1.31×10^{-2} n/s	2.18×10^{-2} n/s	2.64×10^{-2} n/s
60 MeV	1.32×10^{-2} n/s	1.72×10^{-2} n/s	2.62×10^{-2} n/s	3.17×10^{-2} n/s

4.4.2 Applications of intense neutron beam

In nuclear power industry, accurate microscopic neutron reaction data, such as fission and neutron capture cross sections, are essentially required to estimate reactivity and fissile element breeding in the reactor core design. The detailed energy dependence of many of the cross sections is required with a fine energy resolution, in particular for the fine structure resonance of the major fissile, fertile and structural materials. Since

transmutation of minor actinides in spent nuclear fuel is one of the good candidates for reducing volume and radiotoxicity of high-level nuclear wastes, the need for accumulating nuclear data of minor actins increases. High-resolution measurements of microscopic neutron cross-sections demand the most efficient neutron sources covering a wide range of neutron energies. In nuclear physics research, polarized fast neutrons can be used to meet experimental requirements in determining resonance parameter and phase shifts, as well as in searching tiny but important nuclear forces such as the spin-spin interaction or charge symmetry violating mechanisms.

Traditional radioisotope production utilizes reactor neutrons. Since suitable design of target, or surrounding the target with fissile materials for multiplying neutrons may yield higher flux of neutrons than that of reactor neutrons, accelerator-based neutron source can enhance isotope production efficiency significantly. In the non-destructive testing of materials, neutron radiography method has unique advantages in detecting thick and heavy materials over x-ray and γ–ray radiographs. Activation initiated by neutron reactions generates unstable nuclear states or isotopes and the decay channel of them gives characteristic emission signature. The activation technology can be applied to many industrial fields such as quality control in manufacturing, geophysical survey for oil and minerals, and detection of explosives.

Thermal neutrons are one of the most useful probes in condensed matter research such as solids, liquids, polymers, and biological systems. The energy-wavelength relation of thermal neutrons that can match uniquely between the wavelength of the neutron and the interatomic spacings of a solid, and between the energy of the neutron and the characteristic phonon energies in a solid, can be used in studies on structural and dynamical properties of solid. A fact of physics tell us that neutron interacts with a solid primarily by a neutron-nuclear interaction. Different isotopes have different scattering lengths and frequently, different signs of the scattering lengths can be exploited in contrast measurement where the same material is studied, but with one element replaced by its isotope. The scattering efficiency of neutrons by different elements varies irregularly through the periodic table. Investigating structure of high T_c superconducting material may have benefits from neutron probes since their spin and magnetic moment interact very efficiently with magnetic moment of a solid.

4.5 Positron Beam Source

4.5.1 Positron production based on electron accelerator

High-energy photons can produce positrons through pair production in the vicinity of the converter nucleus, elements having high atomic number such as Ta, W, and Pt. Two different processes are available in producing positrons with an electron accelerator. The first one is a direct process; high-energy electrons undergo electron-photon cascades inside the converter, γ-rays from bremsstrahlung initiate pair production. The second one is indirect process based on radiative capture; electron-photon cascades, producing thermal neutrons, initiating radiative capture, for examples, $^{113}Cd(n,\gamma)^{114}Cd$ or $^{63}Cu(n,\gamma)^{64}Cu$, pair production from capture γ-rays. Positron sources can be designed to supply beam intensities up to 10^{10} e$^+$/s.

In the high-energy regime, the total cross-section of positions interacting with a charged particle is almost inversely proportional to its energy. The high-energy positrons should be slowed down in a moderator. Slow, monoenergetic positrons can be produced by implanting fast positrons into a well-annealed sample; within ~100 nm of the surface, the positrons can diffuse back and are ejected nearly monoenergetically by their negative work function. Typical moderator efficiencies are 10^{-4}~10^{-3}. The e$^+$ beam energy is varied electrostatically and the beam is guided by magnetic or electrostatic optical systems onto the surface to be examined. In the low energy regime, the annihilation probability of the slowly moving positron per unit time is proportional to the atomic density and atomic number of the target. The typical lifetime of the positron in Pb is about ~10^{-10} s.

4.5.2 Applications of positron beam

An ideal testing of QED can be performed with positronium together with muonium, since they are a pure leptonic system and the theoretical calculation of its spectrum is unhindered by the presence of heavy particles. In addition to the energy spectrum, the value of the annihilation rates and the fine-structure splitting in the excited states serve as sensitive test of QED predictions. Various ionization processes of atom system can be studied by making use of positron beams such as energy loss spectra, detecting an ion in coincidence with a e$^+$ detecting an ion in coincidence with the ejected e$^-$. Since the positron annihilation can provide the energies for ionization/fragmentation of the molecules, positrons play an important role in investigating various dissociative processes of molecular system.

Measurements of the positron lifetime, the energy distribution, and the angular correlation of the annihilation γ-rays (ACAR) enable one to obtain various information about the behavior of the e$^+$-e$^-$ pair prior to annihilation, and by inference, about the electronic properties of the substance. Positron annihilation technique (PAT) can be

applied in the study of various problems in condensed matter physics and chemistry by making use of fast and slow positrons from radioactive sources for investigating bulk and surface and near surface properties, respectively. Fast positrons lose their energy due to ionizing collisions and phonon scattering and, then, reach to near thermal equilibrium with the solid after penetrating to mean depth of 10~100 μm. In well-annealed crystals of metals and semiconductors, the thermalized positron is in a delocalized state, i.e., a form of a Bloch wave, with peaks at interstitial regions due to core repulsion. On the other hand, the positron in defected material can be trapped in or around low-density regions such as vacancies dislocations and micro cavities. In some liquids and insulating solids, the positron can form positronium by capturing and electron and then the positronium annihilates subsequently by emitting a characteristic γ–rays.

In semiconductor physics research, high precision 2D ACAR data enables one to have information of the anisotropic momentum distribution of the conduction and valence electrons in single crystal. For metal crystals, the position, shape and size of the Fermi surface can be calculated directly from discontinuities in ACAR spectra. Since single aligned positrons can retain much of their spin orientation on thermalizing, they can be used to determine the spin dependent Fermi surfaces in ferromagnetic and superconducting materials.

In metallurgy, the positron annihilation technique has been used in investigation of defects and defect-related properties in metals and semiconductor. If a positron is trapped in a low-density defect such as a vacancy, the positron annihilates with a somewhat longer lifetime than from the delocalized state because of a lower charge density. The Doppler profile and the ACAR spectrum also show significant changes in the momentum density on positron trapping. Measurement of the change in the positron lifetime spectrum as vacancies are thermally activated upon heating the sample, the value of the vacancy formation energy can be determined. Measurements of the positronium lifetime with varying temperature, pressure and crystallinity can explain physical properties of organic solids such as phase transitions in liquid crystals and in polymers.

Reference

[4.3.1] F.R. Arutyunian and V.A. Tumanian, "The Compton effect on relativistic electrons and the possibility of obtaining high energy beams", Physics Letters 4,

p. 176, 1963.

[4.3.2] R.H. Milburn, "Electron scattering by an intense polarized photon field", Physics Review Letters 10, p. 75, 1963.

[4.3.3] L.D. Landau and E.M. Lifshitz, *Quantum Electrodynamics: Course of Theoretical Physics vol. 4*, Pergamon Press, 1982.

5. Conclusion

We discussed the status and plans of the AQBS project at KAERI. There are several issues to solve in using 352 MHz SPS SC cavities as a main accelerator in this project. Although the 2 MeV injector system is operational, the modification of RF cavities in the injection system (change of RF frequency from 180 MHz to 176 MHz) is inevitable. Another issue is the modifications of the HOM couplers and the power coupler (if necessary) of 352 MHz SPS SC cavities in order to adapt two different operation modes. These problems are under discussion with vendors in Korea and German. Lattice beam line is being re-designed due to increase of the accelerating energy. TRACE3D and PARMELA codes are generally used for these designs.

Challenges toward new area are a necessary step for developments and improvements in science as well as industries. The AQBS project is also one of these challenges. Even though the simulations for beam dynamics and beam quality are not completed at this point, we are sure that usage of 352 MHz SPS SC cavities is the best choice to continue our project. Furthermore, we can develop a wide range of quantum beam sources and provide high quality quantum beams to our users for their researches in science or industry.

서 지 정 보 양 식			
수행기관보고서번호	위탁기관보고서번호	표준보고서번호	INIS 주제코드
KAERI/TR-1626/2000			

제목 / 부제	고도양자빔 이용시설 예비설계

연구책임자 및 부서명	이병철 (한국원자력연구소 양자광학기술개발팀)
연 구 자 및 부 서 명	이종민, 정영욱, 조성오, 유재권, 박성희 (한국원자력연구소 양자광학기술개발팀)

출 판 지	대 전	발행기관	한국원자력연구소	발행년	2000. 7
페 이 지	83 p.	도 표	있음(O), 없음( )	크 기	29.7 Cm.

참고사항	

비밀여부	공개(O), 대외비( ), __ 급비밀	보고서종류	기술보고서
연구위탁기관		계약 번호	

초록 (15-20줄내외)	

초전도 가속기를 사용하는 고도양자빔 이용시설을 설계하였다. 고도양자빔 시설은 고출력 자유전자레이저, 단색 X-선 및 감마선, 중저에너지 전자빔, 대출력 펄스 중성자빔, 단색 양전자빔등, 기초과학과 산업분야의 다양한 연구에 이용될 수 있는 광양자 및 입자빔을 발생시키는 시설이다. 고도양자빔 이용시설의 설계는 CERN의 LEP가속기 해체후에 SPS 초전도가속기를 사용하는 것을 전제로 수행되었다.

주제명키워드 (10단어내외)	초전도 가속기, 자유전자레이저, 고도 광양자빔, 전자빔, 감마선, x-선, Compton back scattering, 중성자

BIBLIOGRAPHIC   INFORMATION   SHEET

Performing Org. Report No.	Sponsoring Org. Report No.	Stamdard Report No.	INIS Subject Code
KAERI/TR-1626/2000			

Title / Subtitle	Preliminary Design of the Advanced Quantum Beam Source

Project Manager and Department	Byung Cheol Lee (Lab. for Quantum Optics)
Researcher and Department	Jongmin Lee, Young Uk Jeong, Sung Oh Cho, Jaegwon Yoo, Seong Hee Park (Lab. for Quantum Optics)

Publication Place	Taejon	Publisher	KAERI	Publication Date	July, 2000
Page	83 p.	Ill. & Tab.	Yes(◯), No ( )	Size	29.7 cm.

Note	

Classified	Open(◯), Restricted( ), ___ Class Document	Report Type	Technical Report

Sponsoring Org.		Contract No.	

Abstract (15-20 Lines)

The preliminary design of the Advanced Quantum Beam Source based on a superconducting electron accelerator is presented. The advanced quatum beams include: high power free electron lasers, monochromatic X-rays and γ-rays, high-power medium-energy electrons, high-flux pulsed neutrons, and high-flux monochromatic slow positron beam. The AQBS system is being re-designed, assuming that the SPS superconducting RF cavities used for LEP at CERN will revived as a main accelerator of the AQBS system at KAERI, after the decommissioning of LEP at the end of 2000. Technical issues of using the SPS superconducting RF cavities for the AQBS project are discussed in this report. The advanced quantum beams will be used for advanced researches in science and industries.

Subject Keywords (About 10 words)	Superconducting Accelerator, Free-electron laser, Advanced quantum beam, Electron beam, Gamma-ray, X-ray, Compton back scattering Neutron beam